UNIVERSITÀ DEGLI STUDI DI PADOVA

University of Padova

Department of Surgery, Oncology and Gastroenterology

PhD SCHOOL IN

CLINICAL AND EXPERIMENTAL ONCOLOGY AND IMMUNOLOGY

XXX CYCLE

IMAGING AND RADIOIMMUNOTHERAPY OF PANCREATIC CANCER

Director of the School: Prof. Paola Zanovello

Supervisor: Prof. Antonio Rosato

Co-Supervisor: Dr.ssa Laura Melendez Alafort

PhD Candidate: Mohamed Abozeid

Index

Summary

Pancreatic cancer is a highly lethal disease and the fourth most common cause of cancer-related death worldwide. Surgery is the only curative treatment for local tumors; however, most pancreatic cancer patients present in late stages. Consequently, new tools for early diagnosis are an essential requirement. Mesothelin antigen and prostatic stem cell antigen (PSCA) are tumor-associated antigens (TAAs) expressed in many tumors including pancreatic cancer, with merely no expression in normal pancreatic tissue. Supported by results of previous preclinical and clinical studies, anti-PSCA (APSCA) and anti-Mesothelin (AM) monoclonal antibodies (mAbs) were successfully radiolabeled with either positron (β^+) or gamma (γ) emitter radionuclides, but not Technetium-99m (^{99m}Tc), and have been shown capable of detecting pancreatic cancer lesions.

In this work, we developed new target-specific radiopharmaceuticals for pancreatic cancer detection through APSCA and AM radiolabeling with the γ emitter ^{99m}Tc. We directly radiolabeled AM and APSCA with ^{99m}Tc, yielding a high labeling efficiency (LE) of > 97%. We also proved the high stability of radioimmunoconjugates after dilution and against transchelation, features that can be considered good indicators of *in vivo* stability. As diagnostic agents, mAbs must maintain the ability to specifically recognize their targeted TAAs; thus, we demonstrated that radiolabeling did not interfere with the ability of mAbs to recognize the specific TAAs on tumor cells.

Additionally, by employing the 1,4,7,10-tetraazacyclododecane-1,4,7,10-tetraacetic acid (DOTA) chelating agent, we were also successful in radiolabeling APSCA and AM mAbs with the beta$^-$ (β^-) emitter Lutetium-177 (^{177}Lu), leading to the generation of radioimmunoconjugates endowed with high LE, high stability and high immunoreactivity *in vitro*. Overall, our results are strongly support the use of APSCA and AM mAbs as novel tools for both imaging diagnostic and effective therapeutic approaches in pancreatic cancer.

Introduction

1. Pancreatic Cancer

Despite recent advances in conventional chemotherapy, radiotherapy and early surgical interventions, pancreatic cancer remains a highly lethal disease. Currently, it is the thirteenth most common cancer worldwide and the fourth cause of cancer death in both sexes[1]. The 5-year overall survival (OS) of pancreatic cancer is about 5%, diagnosis in early stages is less than 20% and the most common causes of death are local recurrence and secondary metastasis[2].

Both environmental and genetic factors contribute in the development of pancreatic cancer; the most common factors include smoking, alcohol intake, obesity, long duration type-2 diabetes mellitus and chronic pancreatitis[3].

Pancreatic tumors are classified according to histological origin into endocrine and exocrine tumors; the second group is more common representing 95% of all pancreatic tumors. Pancreatic ductal adenocarcinoma (PDAC) is the most common pancreatic cancer, representing 90% of all pancreatic exocrine tumors[1].

PDAC is a molecular heterogeneous disease with complex genetic mutations; more than 60 genetic mutations including 12 mutations considered core signal pathway were found in 66% of patients[4]. In addition, PDAC originates not only from ductal cells but also from acinar cells after undergoing metaplastic changes into ductal-like cells[4]. Therefore, PDAC has several clones with high genetic diversity and so different responses to conventional treatment[5,6].

Clinical presentation and assessment

Most pancreatic cancer patients complaint of unspecific manifestations; patients commonly present with epigastric pain radiating to the back, unexplained weight loss, jaundice, clay stool and in some cases migratory thrombophlebitis, which is known as Trousseau's

syndrome[3]. Abnormal presentations can be also represented by newly diagnosed diabetes mellitus type-2, chronic pancreatitis and depression[7].

High levels of Carbohydrate antigen 19-9 (CA 19-9) are noted in 80% of patients with advanced stages, it is an important prognostic factor reflecting tumor burden and guides to treatment decision[8]. Multi-detector computed tomography (CT), magnetic resonance imaging (MRI) and ultrasonography (US) can detect pancreatic cancer; CT and MRI are more accurate specially in deciding surgical intervention in border-line locally advanced tumors[8]. Till now, Positron emission tomography (PET)/CT scan has no role in staging and deciding surgical intervention, ongoing clinical trials currently search for its role in pancreatic cancer[8].

Treatment of pancreatic cancer

Surgery is the only curative treatment of pancreatic cancer in early stages. However, only 20% of patients present with localized resectable tumors; besides, post-operative survival rate remains low[9]. Resectability of pancreatic cancer depends on several factors, including general condition, performance status (PS), tumor size, tumor location and staging[1].

Chemotherapy is not a curative treatment in metastatic or advanced pancreatic cancer; its potential palliative benefit should be carefully weighed against its toxic effects. Several regimens have been applied in pancreatic cancer such as gemcitabine (GEM) monochemotherapy, GEM/NAB-paclitaxel, capecitabine/oxaliplatin (XELOX) and FOLFIRINOX[1]. Despite the high toxic profile, FOLFORINOX currently achieves the best anti-tumor response and OS in comparison with other regimens, especially as neo-adjuvant treatment in locally advanced stages[10]. Neo-adjuvant chemotherapy tends to sterilize extended tumor infiltrations and to decrease tumor volume. However, chemotherapy regimens usually induce insufficient anti-tumor responses due to the intense desmoplastic stroma that acts as a barrier to chemotherapy[11].

Radiotherapy has been used as a palliative treatment in unresectable tumors, but is not expected to have significant impact on OS[1]. Recently, modern radiation delivery techniques such as intensity-modulated radiation therapy (IMRT), permit dose escalation to the tumor

and spare the surrounding healthy tissues. IMRT can be applied as an adjuvant treatment and also for metastatic sites[3].

2. Tumor microenvironment of pancreatic cancer

Tumor microenvironment is a dynamic network containing several components of cancer cells, tumor parenchymal cells, dense inflammatory cells and extracellular matrix (ECM)[12,13]. In tumor microenvironment, there are two opposite actions; the tumor inducing immune response and the tumor pro-inflammatory immune response[14]. In tumor microenvironment, cancer cells release cytokines that can modify microenvironment structure and behavior, meanwhile non-cancer cells secret cytokines and growth factors affecting both tumor growth and behavior such as invasion and metastasis.

In pancreatic cancer, fibroblasts in ECM turn into myofibroblasts via transforming growth factor-β (TGF-β). Therefore, ECM of pancreatic cancer is formed of hypovascular densely fibrotic stroma with relatively low cellular content, and infiltrated with pro-inflammatory cells[2,15]. In addition, ECM myofibroblasts produce collagen-1 that contributes in gene expression regulation and cell signal pathways of several functions as apoptosis and malignant cells invasion[16].

Hypovascularity of ECM in pancreatic cancer stimulates the release of both hypoxia inducible factor-1 α and sonic hedgehog; this leads to activation of epithelial mesenchymal transition (EMT). EMT enhances down regulation of tight junction proteins thus stimulating the invasiveness of malignant cells[17]. In addition, hyaluronan which is densely expressed in pancreatic cancer ECM enhances EMT[18]. In a clinical trial, a regimen of GEM and a degrading hyaluronic acid drug (hyaluronidase) improved anti-tumor response in pancreatic cancer patients[19].

Therefore, the pathological nature of pancreatic cancer ECM interferes with systemic chemotherapy and immunotherapy distribution in tumor mass.

TAAs of pancreatic cancer

Several studies pointed out the presence of antibodies in cancer patient sera binding to specific autologous cellular antigens known as TAAs. TAAs are cellular proteins on tumor cells and some normal cells, which can stimulate humoral immune responses towards the tumor[20]. TAAs are characterized by an abnormal expression on tumor cells, such as aberrant regulation and/or overexpression and can be classified into oncofetal antigens, cancer/testis antigens, differentiation antigens and altered antigens[21,22].

Oncofetal antigens are proteins normally expressed in embryonic life with no expression in adult tissues[23]. In normal adults, expression of cancer/testis antigens is restricted to germ line cells in testis, but in malignancy the gene regulation is disrupted and cancer/testis antigens are also expressed in somatic tissues[24]. Differentiation antigens are protein derivatives expressed on tumor cells and their corresponding healthy tissues, such as carcinoembryonic antigen (CEA) expressed in colorectal cancer (CRC) and other epithelial cells of gastrointestinal tract (GIT)[25]. Altered cell surface TAAs are glycolipid and glycoprotein antigens, which are highly expressed in several tumors including pancreatic cancer. Altered cell surface TAAs enhance direct invasion of malignant cells and increase the possibility of metastasis.

Detecting TAAs on tumor cells could be helpful in understanding the molecular changes and pathophysiological pathways leading to tumor development and progression. In addition, TAAs and anti-TAAs autoantibodies could represent diagnostic biomarkers especially in early stages and for the presence of micrometastasis, and could also be used as therapeutic markers to assess tumor response after treatment[26].

Several TAAs are expressed in pancreatic cancer, such as CA 19-9, secreted glycoprotein acidic and rich in cysteine (SPARK), mesothelin antigen and PSCA.

CA 19-9 is the only Food and Drug Administration (FDA) approved pancreatic cancer biomarker since 1980s for recurrence and progression[27,28], while SPARK is a micro-environmental glycoprotein heavily expressed in malignant pancreatic ECM, and its expression is associated with poor prognosis[29].

Mesothelin antigen is a cell surface glycoprotein expressed mainly in mesothelial cells with low expression in upper air way tract, renal system and female reproductive system[30]. Mesothelin is densely expressed in many tumors including lung cancers, gastric carcinoma and triple negative breast cancer. It is also expressed in pancreatic cancer with no expression in normal pancreatic tissue[30-33]. AM mAb targeting mesothelin antigen was able to detect primary and metastatic lesions of pancreatic cancer when labeled with Zirconium-89 (^{89}Zr) in mice model, or Indium-111 (^{111}In) in a clinical trial[34,35].

PSCA is a glycosylphosphatidylinositol (GPI) cell surface protein that belongs to Thy-1/Ly-6 family and has a wide variety of physiological functions. PSCA is present in different systems including renal system, skin, GIT system and placenta[36,37]. Originally, PSCA was identified in prostate cancer but additional studies demonstrated its expression in different tumors as bladder cancer, renal cell carcinoma (RCC) and ovarian cancer[36]. Moreover, PSCA is expressed in the majority of pancreatic tumors with merely no expression in normal pancreatic tissue[38]. In preclinical studies of pancreatic cancer, the role of APSCA was pointed out as new diagnostic tool and effective therapy[39].

PSCA and claudin-4 antigens had been studied as new diagnostic targets for pancreatic cancer in mice model. Anti-claudin-4 or APSCA mAb radiolabeled with γ emitter Iodine-125 (^{125}I) targeted these antigens, while Gamma scintigraphy and single photon emission tomography – CT (SPECT-CT) were used for imaging. Biodistribution results showed tumor uptake with good tumor/background ratio, and this suggested the possibility of targeting these antigens in future for therapeutic purposes[40].

3. Immunotherapy

Immune system has the ability to detect TAAs and to develop a defense immune reaction. However, by time tumor develops immune regulatory circuits with immune-suppressive effect on tumor environment interfering with the anti-tumor response[41]. Studying the interactions between tumor and immune system helps in understanding the immune regulatory circuits that stimulate tumor tolerance[41,42]. Immunotherapy is a cancer treatment

with less toxicities than conventional chemotherapy, and is aimed at modulating the host immune system to fight against cancer[41].

Immunotherapy can be categorized into active immunotherapy and passive immunotherapy; stimulation of anti-tumor immune response is the active immunotherapy, while feeding the tumor microenvironment with adjuvants such as interleukin-2 (IL-2) and tumor necrosis factors (TNF) is the passive immunotherapy. For many years, utilizing the immune system to treat cancer was a complicated process that did not show impressive outcomes. Nowadays, immunotherapy has shown highly satisfactory clinical results in patients with advanced cancers, in particular in those treated with mAbs.

MAbs

MAbs can specifically target TAAs expressed on malignant cells and spare healthy tissues; thus mAbs are useful as diagnostic tools and therapeutic agents in cancer management[43]. In 1993, the first murine mAb was approved by FDA[44]. Since then, more than 20 mAbs have been approved in cancer management[45] (Table 1). In the beginning, murine mAbs induced immunogenicity interfering with wide use in many tumors; patients suffered from severe immunoreaction and mAbs had short-half-lives[46]. By time, chimerization and humanization technologies led to the development of less toxic mAbs[47]. In addition, advanced molecular engineering technologies have allowed modifying mAbs molecular size, binding affinity and specificity[46]. To date, humanization and human mAbs are currently the most suitable technologies to produce mAbs in clinical field.

MAb	Type	Target antigen	Clinical indication
Blinatumomab	Mouse bi-specific T-cell engager	CD3/CD19	Relapsed/refractory B-cell precursor acute lymphoblastic leukaemia, philadelphia chromosome-negative.
Ofatumumab	Human IgG1	CD20	CLL received no treatment.
Obinutuzumab	Humanized IgG1	CD20	CLL received no treatment or with no response to chemotherapy.
Rituximab	Chimeric human-murine IgG1	CD20	CD20 positive diffuse large B-cell NHL, CD20 positive low grade follicular B-cell NHL and CLL.
Yttrium-90-labeled Ibritumomab tiuxetan	Murine IgG1	CD20	Relapsed or refractory low-grade follicular or transformed B-cell NHL.
Brentuximab vedotin	Chimeric IgG1	CD30	Relapsed Hodgkin's lymphoma and relapsed systemic anaplastic large cell lymphoma.
Daratumumab	Human IgG1	CD38	Multiple myeloma after at least three lines of treatment.
Alemtuzumab	Humanized IgG1	CD52	CLL
Elotuzumab	Humanized IgG1	CD319	Multiple myeloma after at least three lines of treatment.
Cetuximab	Chimeric human-murine IgG1	EGFR	KRAS wild-type CRC, locoregional and/or metastatic SCCHN and combination with radiotherapy SCCHN.
Panitumumab	Human IgG2	EGFR	Progressed EGFR-expressing metastatic CRC disease after fluoropyrimidine, oxaliplatin and irinotecan chemotherapy.
Necitumab	Recombinant human IgG1	EGFR	1st line combined with gemicitabine and cisplatin and in metastatic squamous NCSLC.
Pertuzumab	Humanized IgG1	HER2	HER2-positive, early stage or inflmmatory breast cancer, combined with chemotherapy and trastuzumab.
Trastuzumab	Humanized IgG1	HER2	HER2-positive breast cancer and HER2-overexpressing metastatic gastric and gastroesophageal junction cancer.
Trastuzumab emtansine	Humanized IgG1	HER2	HER2-positive, metastatic breast cancer received trastuzumab and a taxane.
Ramucirumab	Recombinant human IgG1	VEGF-R2	Metastatic CRC after progression on bevacizumab and chemotherapy regimen, metastatic NSCLC after progression and advanced gastric or gastroesophageal junction adenocarcinoma.
Bevacizumab	Humanized IgG1	VEGF-A	Recurrent epithelial ovarian, fallopian tube, recurrent or metastatic cervical cancer and primary peritoneal cancer, metastatic CRC, metastatic RCC and advanced NSCLC.
Denosumab	Human IgG2	RANK-L	Unresectable giant tumour of bone and bone metastases from solid tumors to prevent skeleton-related events.
Dinutuximab	Chimeric human-murine IgG1	GD2	High risk neuroblastoma pediatric patients.

Ipilimumab	Human IgG1	CTLA-4	Unresectable or metastatic melanoma.
Nivolumab	Human IgG4	PD-1	Metastatic squamous and non-squamous NSCLC after progression, unresectable or metastatic melanoma and advanced RCC.
Pembrolizumab	Humanized IgG4	PD-1	Metastatic melanoma and NSCLC.

CLL, chronic lymphocytic leukemia; NHL, non-Hodgkin´s lymphoma; EGFR, epidermal growth factor receptor; SCCHN, squamous cell carcinoma of head and neck; NSCLC, non-small cell lung cancer; HER2, human epidermal growth factor receptor-2; VEGF-R2, vascular endothelial growth factor receptor-2; RANK-L, Receptor activator of nuclear factor kappa-B ligand; CTLA-4, cytotoxic associated T lymphocyte protein 4; PD-L1, programmed death ligand 1.

Table 1. MAbs approved for hematological and solid malignancies in clinical field.

MAbs efficacy and safety in cancer treatment vary relying on several factors including TAAs abundance, accessibility, homogeneous distribution and specific expression on tumor cells[48], and their mechanism of action can be divided into immune system independent and dependent mechanisms. Independent mechanisms include induction of a death signal on the target tumor cells and activation of signals blocking or preventing cell growth, while the dependent mechanisms act via stimulating anti-tumor immune responses, antibody-dependent cellular cytotoxicity (ADCC) and complement mediated cytotoxicity (CMC)[43].
In different tumors, mAbs provided a synergetic action with conventional chemotherapy and currently many regimens include both mAbs and chemotherapy agents[49,50].

4. Radioimmunoconjugates

Radionuclides

The selective delivery of radionuclides has always been a promising approach in diagnosis and treatment of cancer relying on their radioactive decay.
Radiations emitted by radionuclides can be used to detect the function and/or anatomical site of targeted tumor; in addition, utilizing the cytotoxic effect of the emitting particles they can be also used in cancer treatment. Apart from Fluorine-18 (^{18}F) and *I, the most important radionuclides in clinical field are radiometals[51] (Table 2).

Depending on their decay, radionuclides can emit particles such as alpha (α) and β particles and/or photons of different energies and qualities. The monoenergetic helium nuclei emitted from nucleus during decay are known as α particles; they have a very short range in tissues (<100 μm, equivalent to a few cell diameters) but a high linear energy transfer (LET) and a high relative biological effectiveness. Consequently, only few doses of α particles are enough to induce the targeted cytotoxic effect[52,53].

Electrons emitted from nucleus are known as β^- particles that are characterized with a relatively high LET. Higher energy β^- emitters kill cells in a longer path-length through the crossfire effect, as it will be mentioned later. However, the lower energy β^- emitters have a high probability to hit DNA, and are therefore considered more cytotoxic[54]. When a β^+ particle is emitted from nucleus, it encounters an electron and annihilates generating two photons in two opposite directions, each one with an energy of 511 keV. Therefore, β^+ emitters are used in PET scan.

Sometimes, in order to get rid of excessive energy, electron shells are rearranged producing low-energy Auger electrons that have just a one cell diameter range. Therefore, Auger electron emitting radionuclides have to be in a close contact with the patient to induce the desired cytotoxic effect [55]. In contrast, γ photons emitted from excited nuclei are massless and thus have a very long range and high penetration to body organs.

Isotope	Half-life	Decay	Gamma (keV)
Fluorine-18	109.77 m	β+ (97%), ec (3%)	511
Gallium-67	3.26 d	Ec	93 (39%), 185 (21%), 300 (17%)
Rubidium-82	1.27 m	β+	511
Nitrogen-13	9.97 m	β+	511
Technetium-99m	6.01 h	IT	140
Indium-111	2.80 d	Ec	171 (90%), 245 (94%)
Iodine-123	13.3 h	Ec	159
Xenon-133	5.24 d	β−	81
Thallium-201	3.04 d	Ec	69–83 (94%), 167 (10%)
Yttrium-90	2.67 d	β−	
Iodine-131	8.02 d	β−	364

IT, isometric transition; ec, electron capture

Table 2. List of common radionuclides used in oncology.

Radiolabeling

In the clinical field, radionuclides are conjugated to peptides or mAbs for diagnostic and therapeutic purposes. The first step in radiolabeling is mAb selection according to its preferential localization in the targeted tumor and/or involvement in a specific physiological function[56]. Then, mAb is labeled with a radionuclide that emits radiation to kill malignant cells and/or detect tumor site and its physiological activity. After being radiolabeled, mAb binds to its specific TAA expressed on malignant cells.

Various requirements should be considered before radiolabeling. Radionuclides are selected by consideration of both the radiophysical properties and the LE. The half-life of radionuclide should match the biological half-life of the conjugated peptide; for example, radionuclides with shorter half-lives than the conjugated peptide will lose radioactivity before reaching the target, while others with longer half-lives will reach low dose radioactivity to the targeted tumor[57]. Several essential properties of mAbs are also required when selected for radiolabeling, as the high binding affinity for TAA, high specificity, high tumor to background ratio, low immunoreactivity and high metabolic stability[58]. It is remarkable to mention that tumor factors such as size, site and heterogeneity of TAAs expressed on malignant cells should also be taken into account during choosing the appropriate radioimmunoconjugate.

For example, large tumors should be targeted using a radionuclide emitting long range particles, while small primary and distant small metastases could be treated using a radionuclide emitting medium range β^- or α particles[55]. The heterogeneous distribution of TAAs could be overcome using labeling methods to achieve high specific activity labeled mAbs and radiometals with long range radiation emission. Finally, important considerations related to *in vivo* behavior of the final radiometal complex are required including Redox properties, charge, stability, stereochemistry and lipophilicity[59].

MAbs labeling usually involves two main strategies: direct labeling, and indirect labeling. The direct labeling is a simple and rapid method; this approach mostly uses oxidizing or reducing agents to generate electrophilic species of the radioactive atoms, which then react with functional groups on the protein. Direct labeling is a preferable method for mAb or its fragments, while it is difficult to be applied for smaller biomolecules contain few or no disulfide bonds, as any change in the disulfide bonds would affect their biological properties[60]. Technetium pertechnetate ($^{99m}TcO_4^-$) can be reduced in one step using several reducing agents including Tin (II) chloride ($SnCl_2$), borohydride dithionite and hydroxamine. Reducing agent $SnCl_2$ converts mAbs disulfide linkages into free thiols and allows strong binding to ^{99m}Tc. Although it has some disadvantages as colloids ($^{99m}TcO_2/SnO_2$) formation, Tin (II) is mostly used in commercial kits, as its rapid reduction kinetics provides a quick preparation of radiopharmaceuticals. Subsequently, a weak chelating agent is required to stabilize Tin (II) and ^{99m}Tc in its intermediate oxidation state[60].

MAb-based radiopharmaceuticals indirectly labeled with radiometals consist on four moieties; the TAA-targeting mAb, the spacer, a bifunctional chelating agent (BFCA) and the radiometal[51]. The spacer is used to separate BFCA and mAb, thus avoiding the influence of BFCA on mAb binding affinity to TAA. Moreover, the spacer improves the radiopharmaceutical pharmacokinetics and increases its hydrophilicity[51]. The chelation chemistry evolution has enabled using new metal radionuclides with different radioactive properties in various clinical situations[61]. Selection of BFCA relies on the chemical properties of the required radiometal. BFCAs are small molecules mostly derived from polyaminocarboxylic acids with a conjugation group for radiolabeling and a binding unit for

attachment to the protein. BFCAs molecules can be covalently conjugated to the protein (e.g mAb) through their reactive sulfhydryl or amino groups forming an amide bond[51,62] and their advantage is that mAb chemical modification will be separated from the addition of radionuclide[62]. BFCA efficiently coordinates the radiometals with all the amino groups and some carboxyl groups; these multiple bonding sites provide high binding strength[62]. In general, BFCAs compete with the natural chelators present in bloodstream (e.g. serum albumin and transferrin). Therefore, the physiochemical properties of radiometal complexes including BFCA should be kinetically inertness and thermodynamically stable to avoid the undesired biodistribution and so prevent the expected toxic effects on non-targeted organs[51]. Acyclic BFCAs as diethylenetriaminepentaacetic acid (DTPA) have been widely used; DTPA binds to mAb forming an amide bond using one carboxylic group. DTPA derivatives were used with ^{111}In in the first clinically approved radiopharmaceutical octreotide. However, apart from ^{111}In, acyclic BFCAs showed no *in vivo* stability for radiometals[51] and so cyclic BFCAs are more preferable. DOTA is the most commonly used cyclic BFCA, being a kinetically inert complex in comparison with its acyclic analog DTPA[44]. One acetic acid function of DOTA binds to mAb forming an amide group, thus allowing its carbonyl oxygen to bind to the radiometal[51,63]. By time, DOTA derivatives were developed with extra carboxylate arms in one of the nitrogens, this increasing the number of donor atoms available for radiometal binding. DOTA modified forms as DOTA-NHS ester and p-SCN-Bz-DOTA are now available, and the coupling reaction using these modified forms succeeded in cutting the incubation to one-step[62]. Other examples of most commonly used cyclic BFCAs includes 1,4,7-triazacyclononane-1,4,7-triacetic acid (NOTA) that has an optimal small cavity for Gallium $(Ga)^{3+}$ small ion, 1,4,8,11 tetraazacyclotetradecane, 1,4,8,11,tetraacetic acid (TETA) and their derivatives[51] (Fig.1).

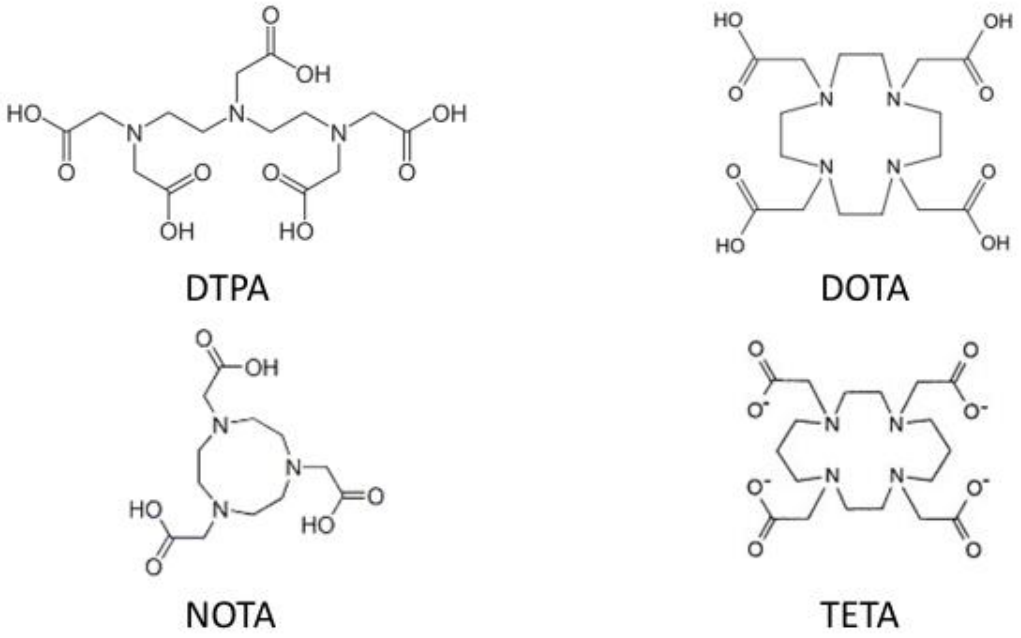

Figure 1. Structures of chelating agents DTPA, DOTA, NOTA and TETA.

Radioimmunodiagnosis

Nuclear scan is the most frequently used diagnostic method in molecular imaging, offering good sensitivity without any depth limit in soft tissues; it is an effective diagnostic tool providing both the anatomical structure and functional information of the tumor, and its radioactivity can be simply detected and measured using external scintigraphy.

MAbs labeling with β^+ or γ emitter radionuclides can be used for PET or SPECT scan, respectively. Both PET and SPECT are a quantitative nano-molar sensitive range scans, as the measured radioactivity is directly proportional to the target molecule concentrations in the tissue.

In PET scan, β^+ emitting radionuclides produce two annihilation γ photons that move in two opposite directions and are received at the same time by the detector. The commonly used radioisotopes in PET scan are ^{18}F, ^{124}I and copper ($^{60/64}Cu$)^{64}. Gamma camera is the most common SPECT system, where γ photons emitted from radionuclides are detected to assess the function and morphological characterization of the tumor. Gamma camera consists of a detector coupled with an imaging sub-system such as an array of Photo-Multiplier tubes

(PMT) and associated electronics. The detector is a single large thallium-doped sodium iodide (NaI) (Tl) scintillation crystal. Collimators of gamma camera form an image on the crystal, accept perpendicular photons and reject off-axis photons that degrade the image (Fig.2). Total body penetration of γ rays enables whole-body non-invasive scans in three dimensional (3D) manner, allowing quantitative analysis of tracer pharmacokinetics and distribution[65,66]. Therefore, these techniques have been used for early disease detection and real-time monitoring of therapeutic responses, as well as for investigating drug efficacy with optimal results[67].

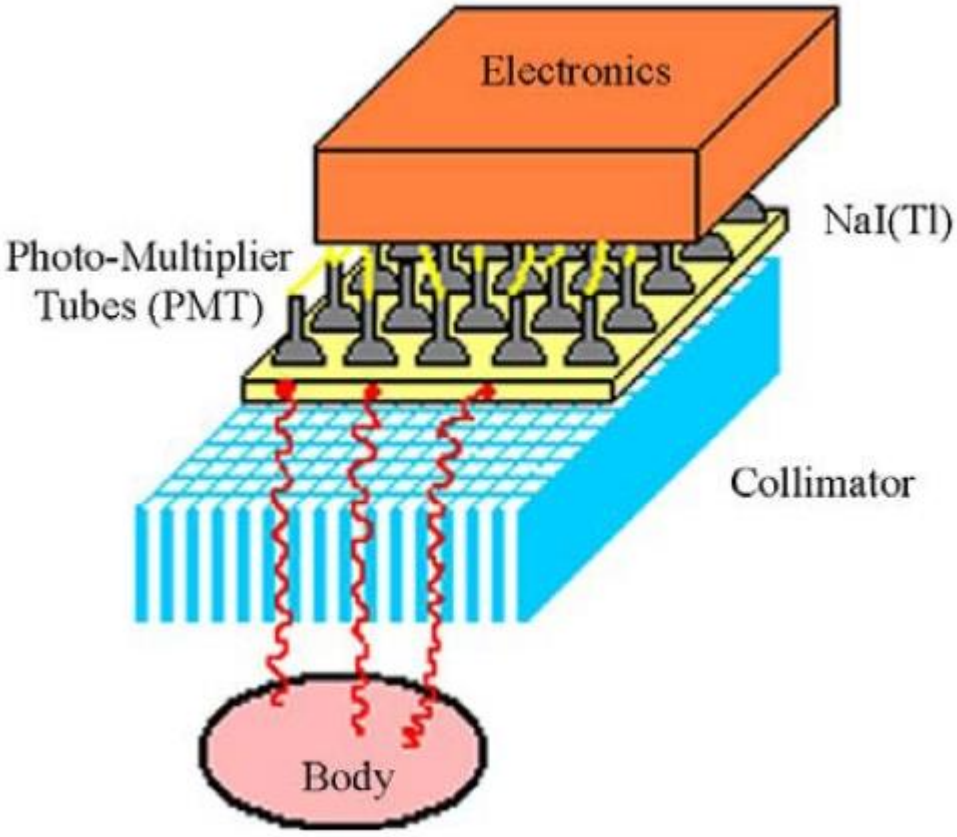

Figure 2. Elements of a gamma camera; Collimator, PMT, TI.

Radionuclides produced via generators are less expensive when compared with accelerator or reactor produced radionuclides[59]. ^{99m}Tc is the most commonly used radioisotope for preclinical studies and clinical practice, it is produced from the parent Molybdenum-99 (^{99}Mo) (half-life: 2.78 days) in the ^{99}Mo/^{99m}Tc generator. ^{99m}Tc pharmaceuticals are commonly used to diagnose cancer of different organs; ^{99m}Tc has ideal nuclear properties, low cost with

optimal monoenergetic (140 keV) γ photons for SPECT scan, thus providing a high resolution imaging[68,69]. In addition, ^{99m}Tc has a relatively short half-life (6 h), which is appropriate for radiopharmaceutical preparation and helps in avoiding delivery of unnecessary radiation to the patient[70]. Another breakthrough was the production of commercial kits of the radiopharmaceuticals precursors (non-radioactive freeze dried kits) with long store period duration.

Radioimmunotherapy (RIT)

RIT has emerged as an attractive and promising strategy for the management of malignant diseases. RIT is a targeted treatment using radionuclides to augment mAbs efficacy; when mAbs are labeled with α or β^- radionuclides, they emit ionizing radiation that travels a short distance and concentrates in the tumor area. The irradiated malignant cells absorb high amounts of energy, and this provokes direct macromolecular damage, produces oxygen free radicals [71] and leads to cell apoptosis and/or programmed necrosis[72,73].

As mentioned before, the appropriate radionuclides should be selected relying on several factors including tumor size and type to produce the maximal therapeutic effect. While β^- emitter radionuclides (e.g ^{177}Lu, 0.8 MeV) can travel only 2.0-4.0 mm, the high energy β^- emitters (e.g ^{188}Re, 2.1 MeV) transverse up to 11 mm and so are more cytotoxic for distant cells[54]. Therefore, uniform binding of radiolabeled mAbs is not a prerequisite as the relative wide range of ionization can damage cells in proximity to those that are not directly bound by the mAb; this is known as the cross-fire effect[53].

RIT affords some potential benefits over external beam conventional radiotherapy; it has the ability to deliver radiation to the tumor more precisely, delivers radiation to metastatic sites and affects tumors with heterogeneous expression of targeted TAAs. In addition, while external beam conventional radiotherapy delivers as a high burst radiation dose divided into fractions over several weeks, RIT administered intravenously provides lower doses of radioactivity. Moreover, RIT has a higher tumor uptake than conventional radiation; it is also noteworthy to mention that RIT absorbed doses retained in tumor for several weeks

depending on the physical half-life of radionuclides and the biological half-life of mAbs[54]. Therefore, low doses of RIT could induce lethal effects as compared with high doses of conventional radiotherapy, and thus avoiding excessive radiation exposure.

The most common β^- emitters currently used in RIT include ^{131}I, Yttrium-90 (^{90}Y) and ^{177}Lu, the latter being a reactor-produced radionuclide through irradiation of enriched ^{177}Lu. ^{177}Lu has a half-life of 6.75 days, emits two γ emissions (6.4% at 113 keV and 11% at 208 keV) and three β^- emissions (12% at 0.176 MeV, 9% at 0.384 MeV, and 79% at 0.497 MeV) [60]. The maximum particle range of ^{177}Lu is between 2-4 mm and so it is more applicable for RIT of small primary and metastatic lesions[74]. Radiolabeling with ^{177}Lu is carried out at pH 4-5 to avoid formation of insoluble colloidal hydroxides[51]. Meanwhile, ^{90}Y emits β^- particles with higher energies than ^{177}Lu, and has a greater efficiency and higher linear attenuation[75]. Therefore, ^{90}Y is proved more effective for the treatment of large tumors.

The successful development of this approach has resulted in the recent clinical approval of two antibody-radionuclide conjugates for the treatment of NHL, ^{90}Y-labeled ibritumomab tiuxetan (Zevalin®, Biogen, IDEC, Cambridge, MA) and ^{131}I-labeled tositumomab (Bexxar®, Corixa, Seattle, WA, USA)[44,76].

The rapid advances in molecular and cellular biology have recently revealed an increasing number of novel potential disease targets and biomarkers, especially those aberrantly expressed in biological malignancies and involved in invasiveness and metastasis. Consequently, new tools for early diagnosis and therapeutic approaches for pancreatic cancer are imperatively needed.

Aim of the project

This research project aimed at developing new target-specific tools for pancreatic cancer detection and therapy based on radiolabeling of APSCA and AM mAbs.

We validated *in vitro and in vivo* the binding capacity of mAbs to target and detect pancreatic cancer.

A reproducible method to label directly the mAbs with the γ emitter ^{99m}Tc was optimized to obtain radio-immunodiagnostic agents with high radiochemical yield. The ^{99m}Tc-mAbs binding specificity for the antigen receptors and stability of radio-immunodiagnostics agents were assessed *in vitro*.

MAbs were also radiolabeled by indirect method using the chelating agent DOTA and the β^- emitter ^{177}Lu, to obtain a teragnostic agent for pancreatic cancer. The number of DOTA conjugated to each mAb molecule was quantified, and the binding specificity of DOTA-mAbs conjugates for the antigen receptor was assessed *in vitro*. Labeling reaction of DOTA-mAbs with ^{177}Lu was optimized to obtain a high radiochemical yield. Finally, stability of ^{177}Lu- DOTA-mAbs conjugates and their binding specificity for the antigen receptors were assessed *in vitro.*

METHODOLOGY

MAbs targeting PSCA and mesothelin were kindly provided by Prof. Marco Colombatti from the Institute of Immunology and Infectious Diseases, University of Verona. All mAbs production batches were analyzed by gel-filtration chromatography to probe their purity before to start the experiments.

1. Flow cytometry study

Flow cytometry studies were carried out in order to confirm the ability of both APSCA and AM mAbs to recognize the specific antigen receptors PSCA and mesothelin on the surface of the malignant cells.

1.1 Cell lines

Two tumor cell lines were used, the human pancreatic adenocarcinoma T3M4 cell transduced or not to express PSCA receptors (T3M4-PSCA) and the embryonic human kidney 293-cell transduced or not to express mesothelin receptors (293-Meso). Both cell lines were obtained from American Type Culture Collection (ATCC, USA) and were maintained in RPMI 1640 medium (EuroClone, Italy). Medium was supplemented with 10% heat-inactivated fetal bovine serum (FBS) (Gibco), 1% Ultraglutamine, 1% Hepes buffer and 1% penicillin/streptomycin (all from Lonza, Switzerland).

Cell lines were grown in 25, 75 or 175 cm^2 flasks (Falcon, Becton Dickinson) at 37°C in a humidified atmosphere with 5% CO_2.

1.2 Assessment of *in vitro* binding specificity for the antigen receptor

MAbs binding specificity for the antigen receptors was assessed on cell lines by flow cytometry using a fluorescence-activated cell sorting FACSCalibur (Becton Dickinson, USA). APSCA and AM mAbs were stained with Alexa 680 using the SAIVI rapid antibody labeling kit (Invitrogen, Italy) according to the manufacturer's protocol. The stained mAbs were purified by size exclusion chromatography on a PD10 column. Then, the protein concentration as well as labeling degree were determined by absorbance at 280 and 679 nm.

Cancer cells ($3x10^5$) expressing PSCA or mesothelin antigens were stained by incubation on ice with 1 µg of stained-APSCA or stained-AM mAb for 30 min in the dark, followed by flow cytometry analysis. Cells were washed in Phosphate buffer solution (PBS) (0.01M NaCl concentration and pH 7.4), resuspended in 250 µl PBS and measured the fluorescence on a FACSCalibur. Then, the data collected were analyzed with FlowJo software (TreeStar Inc., Olten, Switzerland) to obtain the geometric mean. The cells auto-fluoresce data were obtained by flow cytometry analysis of untreated cells on the same conditions described before.

1.3 Assessment of *in vivo* binding specificity for the antigen receptor by optical imaging

Optical imaging studies were performed in mice to confirm the ability of both mAbs to identify specifically the antigens *in vivo*. Animal studies were performed in accordance with the ethical guidelines for animal research adopted by the University of Padua, acknowledging the Italian regulation and European Directive 86/609/EEC as to the animal welfare and protection and the related codes of practice.

Tumors were induced in six weeks-old (20 – 25 g) NOG mice (Charles Rivers Laboratories) by subcutaneous injections of 1×10^6 tumor cells. To test the specificity of AM mAb, animals were inoculated on the right side with the 293-Meso cells and in the left side with 293 wild type cells. APSCA specificity for the receptor was tested by inoculation of T3M4 wild type cells on the mice right side and T3M4-PSCA cells on the left side. When the tumor growth was

stabilized, from 7 to 14 days after inoculation, animals were placed on a low manganese diet to reduce autofluorescence from normal mouse chow, and abdominal fur was removed by depilation. Three days later, animals were treated with APSCA or AM mAbs (50 μg) dyed with Alexa 680, administered by tail vein injection. Then, mice were anesthetized to collect fluorescence data with a MX2 (ART, Montreal, QC, Canada) using a total body scan at different time points with a 670 nm laser and a 693 LP filter. The spatial resolution/scan step was fixed at 1.5 mm, exposure time was 0.5 s and laser power was automatically adjusted for each scan session.

2. Direct labeling of mAbs

Direct labeling method reported by Stephen J. Mather et al.[77] represents a simple and rapid procedure to produce radiolabeled mAbs without affecting their immunoreactivity. Therefore, this method is successfully used to label several antibodies in preclinical and clinical trials [78-80].

Before starting the labeling procedure, both APSCA and AM mAbs were analyzed by size exclusion High Performance Liquid Chromatography (HPLC) to determine their purity. Size exclusion HPLC analysis was done using a quaternary pump with the ultra violet (UV) detector set at 280 nm (Agilent, Italy) and interfaced with NaI radioactive detector (Raytest, Gabi star, UK) using a column Zorbax-250 (Aglient, 4 μm-9.4x250 mm) as stationary phase and an isocratic method with a flow rate 1 mL/min, using 0.1 M PBS solution, pH.7 as the mobile phase. Pre-column filters were used at all times.

2.1 Reduction of mAbs

Direct labeling with ^{99m}Tc usually involves the conjugation of reduced ^{99m}Tc to the free thiols generated by reduction of a cysteine bridge [81]. Therefore, the first step was to reduce the mAbs APSCA and AM using 2-mercaptoethanol (2-ME) (Sigma-Aldrich, Italy). To start, mAbs

were concentrated to 10 mg/ml by centrifugation using an Agilent concentrators spin MWCO 30,000 (Sartorius Stedim biotech, Italy). The concentrated solution of APSCA or AM was incubated at room temperature with the reducing agent 2-ME at different molar ratios (mAb:2-ME): 1:500, 1:1000, 1:1500, 1:2000, 1:2500, 1:3000, 1:3500 and 1:4000 for 30 min. Then the reaction mixture was purified by agilent concentrators spin MWCO 5,000 (Sartorius Stedim biotech, Italy) to eliminate the 2-ME, and the samples were analyzed by size exclusion HPLC to determine mAbs integrity using the method described above.

The number of free sulfhydryl groups formed by the reduction of APSCA and AM were quantified using Ellman's reaction test as follows: 50 µl of reduced mAbs was mixed with 50 µl of a solution containing 0.3 mg/ml of 5,5'-Dithio-bis-(2-nitrobenzoic acid) Ellman's Reagent (Sigma-Aldrich, Italy) and diluted to 3 ml with 0.1 mol/L sodium phosphate, pH 8.0. Then, the mixture was incubated for 5 min at room temperature and the color change was measured using UV-Vis spectrophotometer at 409 nm. Thiols number was quantified by comparison with a standard curve obtained with a series of cysteine solutions ranging from 0.25 to 1.0 mmol/L.

2.2 Labeling of mAbs with Technetium-99m (^{99m}Tc)

APSCA and AM were radiolabeled using a direct method by the addition of $^{99m}TcO_4^-$ solution eluted from ^{99}Mo/^{99m}Tc generator (Mallinckrodttm, Austria), 0.5 mM etidronic acid solution (EHDP) (Sigma-Aldrich, Italy) and 0.1 M $SnCl_2$ solution (in 0.1 M HCl) to a vial containing 200 µg of the reduced APSCA or AM. The samples were stirred gently and incubated at room temperature. In order to optimize the formulation and to obtain the highest LE, the following parameters were examined: the volume of $^{99m}TcO_4^-$ solution (100, 200, 300 and 500 µL); the amount of $SnCl_2$ (0.5, 1, and 2 µg); the amount of EHDP (0.5, 2, 5 and 10 µg) and the incubation time (10, 15, 30, and 60 min), maintaining always the final volume of the reaction mixture between 0.75 to 1 ml to ensure that the reagents concentration was high enough to react.

Due to ^{99m}Tc-EHDP could be obtained as radiochemical impurity in the reaction mixture; EHDP was radiolabeled by incubation with $SnCl_2$ and $^{99m}TcO_4^-$ solution and analyzed by size exclusion HPLC to be used as control.

2.3 Stability studies of ^{99m}Tc-labeled mAbs

Dilution stability

To determine the stability of radiolabeling mAbs after the dilution, 100 µL of ^{99m}Tc-AM or ^{99m}Tc-APSCA were diluted to 1:10, 1:20, 1:50 and 1:100 with 0.9% saline chloride solution (SS) or 0.1 M PBS, pH.7 or to 1:10 and 1:100 in human serum (HS) and incubated at room temperature for 24 h. Radiochemical purity (RCP) was determined at different time intervals up to 24 h by size exclusion HPLC and instant thin layer chromatography analysis (ITLC).

Undiluted ^{99m}Tc-AM and ^{99m}Tc-APSCA were also analyzed at the same time points to be used as controls.

ITLC analysis was performed on silica gel impregnated glass fiber (ITLC-SG) sheets (Gelman, USA) running a sample of 1 µl on 10×1-cm strips using as mobile phases acetone and 0.9% SS. Distribution of radioactivity on the strip was determined by cutting it into 1-cm pieces and each one was counted in a NaI-scintillation counter (LKB Wallac, 1282 Compugamma CS, Turku, Finland). Retention factor (Rf) of ^{99m}Tc-mAbs is 0.0 in acetone and in SS. The Rf of the labeled EHDP is 0.0 in acetone and 1.0 in SS. In both solvents, free $^{99m}TcO_4^-$ migrates to the front (Rf=1.0) and ^{99}Tc-colloid stays at the origin (Rf=0.0). A third system, ITLC-SG sheets impregnated with 5% human serum albumin and NH4OH:ethanol:H2O (1:2:5) as mobile phase, were also used to determine the amount of colloid since it remains at the bottom of the strip while the radiolabeled antibody migrates with the solvent front.

Cysteine challenge assay

Cysteine challenge assay was performed to evaluate the *in vitro* stability of radiolabeled mAbs. The test was carried out by addition of 100 µl of ^{99m}Tc-AM or ^{99m}Tc-APSCA (1 mg/ml)

to a propylene test tube containing a fresh cysteine solution to obtain a mixture solution with different molar ratios (mAb:cysteine), 1:10, 1:100 and 1:1000. The reaction mixture were incubated at 37°C for 24 h and analyzed at time points ranging from 0.5 to 24 h by size exclusion HPLC and ITLC as described before, to determine the percentage of ^{99m}Tc which transchelates from the radiolabeled mAbs to the free cysteine.

^{99m}Tc-AM and ^{99m}Tc-APSCA solutions without dilution were also analyzed at the same time points to be used as controls.

2.4 Assessment of ^{99m}Tc-mAbs binding specificity for the antigen receptor *in vitro*

Binding properties of ^{99m}Tc-labeled AM and APSCA mAbs were assessed by a competition binding assay using 293-Meso and T3M4-PSCA cell lines, respectively. Cells were suspended in fresh RPMI 1640 medium and diluted to a concentration 1×10^6 cells/ml. To a glass test tube containing 1 ml of cell suspension was added 10 µl (1 kBq) of ^{99m}Tc-PSCA or ^{99m}Tc-AM solution. The mixture was vortexed and incubated at 37°C. At 90 min, the tubes were vortexed again, the cells were transferred in Eppendorf microcentrifuge tube (1.5 mL) and centrifugated (3000 rpm for 3 min at 10°C). The supernatant was separated from the pellet and the bottom tip containing the cell pellet was washed twice with 1 ml of 0.1 M PBS, pH.7. The activity in the washed cell pellet was counted using a gamma-counter (Cobra II, Packard) to determine the cell uptake.

To determine the internalization fraction, the ^{99m}Tc-mAb bound to the cells membrane was removed. The washed cell pellet obtained before was incubated with 1mL of saline acetate buffer solution (0.2 M acetic acid/0.5 M NaCl) for 2 min at room temperature, the tubes were then centrifuged (3000 rpm for 10 min at 10°C), the supernatant was separated from the cell pellet and each fraction was placed in a separated counting tube to measure their activity. The pellet radioactivity was considered as the internalized fraction.

The non-specific binding was determined in parallel by incubation of a 10-fold excess of unlabeled antibody 30 min before the addition of the ^{99m}Tc-mAb, to block the cell receptors.

3. Indirect labeling of mAbs

3.1 Conjugation of chelating agent to mAbs

DOTA-mAbs conjugates were prepared as reported in the literature by Forrer et al.[82], in resume, 20 ml of APSCA or AM solution (1 mg/ml) were washed three times with 0.2 M sodium carbonate buffer, pH 9.5 and concentrated by centrifugation using Agilent concentrators spin MWCO 30,000 (Sartorius Stedim biotech, Italy). MAb concentrated solution (100 mg/ml) was then incubated with the chelator DOTA solution (Macrocyclics, USA) at 37°C in a molar ratio of 1:5 (mAb:DOTA). The coupling reaction was quenched by adjusting the pH to 7.0 with 0.25 M ammonium acetate buffer, pH 5.5. The product was washed three times and purified by centrifugation using Ultra-15 filter to remove the excess of free DOTA. Two washes were done with 0.25 M ammonium acetate, pH 7.0 and the last one with SS. Finally the concentration of conjugates was determined spectrophotometrically at 280 nm and the products were diluted in SS at a concentration of 5 mg/ml.

Size exclusion HPLC analysis of final products was performed using the same method reported above. Retention times of DOTA-AM and DOTA-APSCA were compared with those of the AM and APSCA respectively to confirm the DOTA conjugation.

3.2 Quantification of chelating agent number conjugated to each mAb molecule

Matrix-assisted laser desorption ionization mass spectroscopy (MALDI-MS) analysis was performed using a REFLEX time-of-flight instrument (4800 Plus MALDI TOF/TOF, AB Sciex, Framingham, Massachusetts, USA) to determine the average number of DOTA chelators per each mAb molecule. MALDI matrix was prepared as follow; one tube of sinapinic acid (MW: 224.21) was dissolved in 50:50 acetonitrile/water with 0.1% TFA to have a MALDI matrix with a concentration of 10 mg/ml. Then the unconjugated mAbs and immunoconjugates DOTA-

mAb were desalted by washing several times with milliQ water and concentrated to 25 mg/ml by centrifugation at 4ºC. MALDI-MS analysis were perform by mixing the desalt mAbs solutions with the MALDI matrix (in a molar ratio of 1:1) on the sample ground plate and left there until the samples were evaporated completely. Then the metal plate was inserted into the vacuum to run the analysis.

3.3 Assessment of DOTA-mAb binding specificity for the antigen receptor *in vitro*

DOTA conjugation effect to the mAb immunoreactivity was determined measuring the DOTA-mAbs binding specificity for the antigen receptor *in vitro*.

To carry out the binding specificity test, 8 sequential dilutions (from 1000 nM to 0.1 nM) of both DOTA-mAb conjugates in PBS-BSA 0.2% were prepared and added to glass test tubes. Dilutions of both unconjugated-mAbs were prepared at the same time to be used as controls. Then T3M4-PSCA and 293-Meso cells were treated with 0.02% EDTA for 10–15 min at 37ºC, washed three times and re-suspended in the PBS-BSA 0.2%. Next, 0.5 ml of cell suspension was added to glass tubes with the DOTA-mAbs or mAbs serial dilutions, and incubated on ice. One hour later, cells were washed with cold PBS and stained with saturating amounts of an anti-mouse immunoglobulin fluorescein isothiocyanate (FITC)-labeled goat antibody (Becton and Dickinson, Sunnyvale, CA) for 30 min in the dark. After incubation, cells were washed twice again and analyzed by FACS using an Epics XL cytometer (Coulter, Hyaleah, FL) with an exciting wavelength of 488 nm at 200 mW power. The percentage of positive cells and the mean fluorescence intensity values were considered. The results were expressed as percentage saturation of the total stainable antigen sites.

3.4 Labeling of DOTA-mAb with Lutetium-177 (^{177}Lu)

To prepare ^{177}Lu-DOTA-mAbs, 10 µl (≈185 MBq) of $^{177}LuCl_3$ solution (ITG Isotope Technologies Garching GmbH, Germany) was added to the vial with 100 µl of DOTA-APSCA or DOTA-AM solution (5 mg in 1ml of 0.25 M ammonium acetate, pH 7.0). The reaction mixture was stirred

and incubated at 37°C. LE was evaluated at different time points ranging from 15 min to 4 h by size exclusion HPLC and ITLC-SG. ITLC-SG analysis was carried out running a sample of 1 µl on a 10 cm strip of ITLC-SG using methanol as mobile phase. Distribution of radioactivity on the strip was determined as described above. Rf in methanol for $^{177}LuCl_3$ and ^{177}Lu-DOTA-mAbs were 1.0 and 0.0 respectively. Size-exclusion radio-HPLC analyses were carried out as mentioned before.

3.5 Stability studies of ^{177}Lu-labeled DOTA-mAb

Dilution stability

In vitro stability of the purified ^{177}Lu-DOTA-mAbs was determined after dilution of 50 µl of ^{177}Lu-DOTA-APSCA or ^{177}Lu-DOTA-AM conjugate to a ratio 1:10 and 1:100 with both 0.1 M PBS, and SS. Dilutions were incubated at room temperature and then analyzed as described above, at different time points between 5 min and 24 h by size exclusion HPLC and ITLC-SG using methanol as mobile phase.

Stability against transchelation

^{177}Lu-DOTA-APSCA and ^{177}Lu-DOTA-AM were also tested to prove their stability against transchelation in the presence of a competitor for the ^{177}Lu ions. The test was carried out by incubation of 50 µL (≈3 MBq) of purified ^{177}Lu-DOTA-APSCA or ^{177}Lu-DOTA-AM solution (1 mg/ml) with 100 times molar excess of CaDTPA solution (1 ml) at 37°C for 3 days. The reaction mixtures were analyzed at different time points ranging from 0.5 to 72 h by size-exclusion HPLC.

3.6 Assessment of ^{177}Lu-DOTA-mAbs binding specificity for the antigen receptor *in vitro*

Immunoreactivity of ^{177}Lu-DOTA-AM and ^{177}Lu-DOTA-APSCA were determined measuring the binding specificity of radiolabeled mAbs to the 293-Meso and T3M4-PSCA cells receptors *in vitro*. Cells were suspended in fresh RPMI 1640 medium and diluted to a concentration 1×10^6

cells/tube (0.5 ml) then incubated with 10 µL (≈1 MBq) of ^{177}Lu-DOTA-APSCA or ^{177}Lu-DOTA-AM solution (1 mg/ml) in triplicate. The mixture was vortexed and incubated at 37°C for 2 h then the pellet was separated from the supernatant and washed twice with 1 ml of 0.1 M PBS, pH.7. The cell pellet was counted using a gamma-counter (Cobra II, Packard) and considered as the cell uptake.

Non-specific binding was assessed in parallel by incubation of a 10-fold excess of unlabeled mAb 30 min before the addition of the corresponding ^{177}Lu-DOTA-mAb, to block the cell receptors.

RESULTS AND DISCUSSIONS

APSCA and AM mAbs were kindly provided by Prof. Marco Colombatti et al. from the Institute of Immunology and Infectious Diseases of Verona University.

1. Gel-filtration chromatography analysis to native mAbs

To prove the purity of mAbs produced, a gel-filtration chromatography analysis was carried out at the Institute of Immunology and Infectious Diseases. This analysis permits to separate proteins present in a sample based on their size. Smaller molecules diffuse into the pores of the beads and therefore move through the bed more slowly, while larger molecules enter less thus moving through the bed more quickly. At the end of the synthesis and purification processes, analysis showed a single peak for both APSCA and AM, which indicates a single protein; no protein aggregation or degradation was found (see fig. 1 and 2).

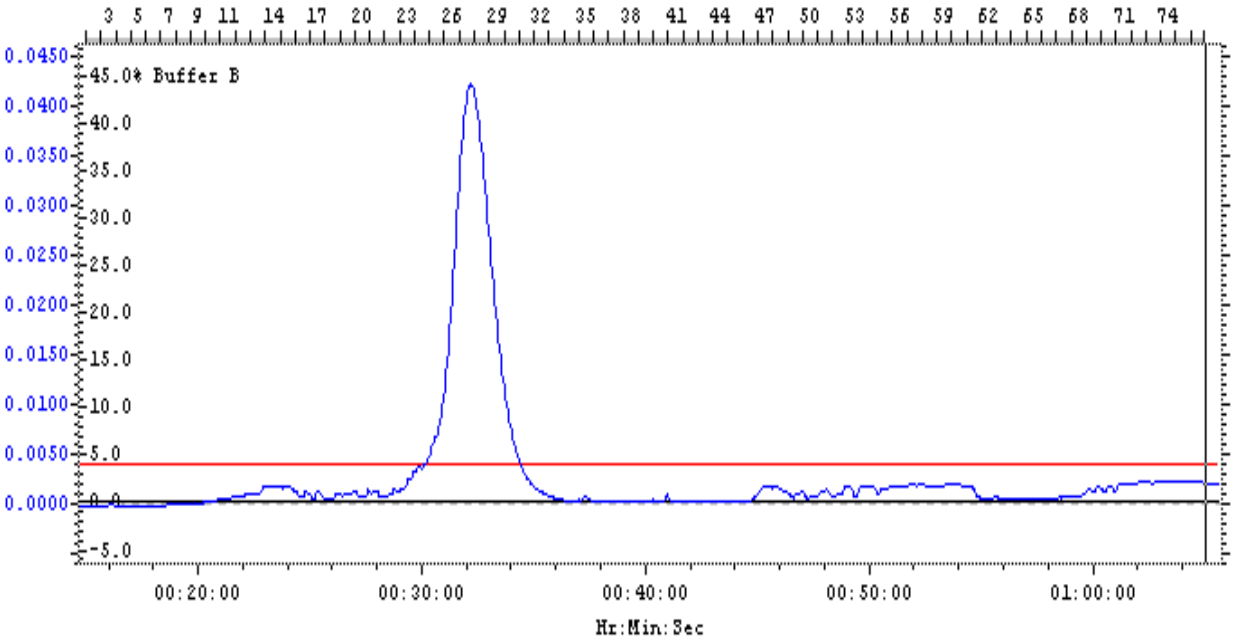

Figure 1. Gel-filtration chromatography analysis of APSCA.

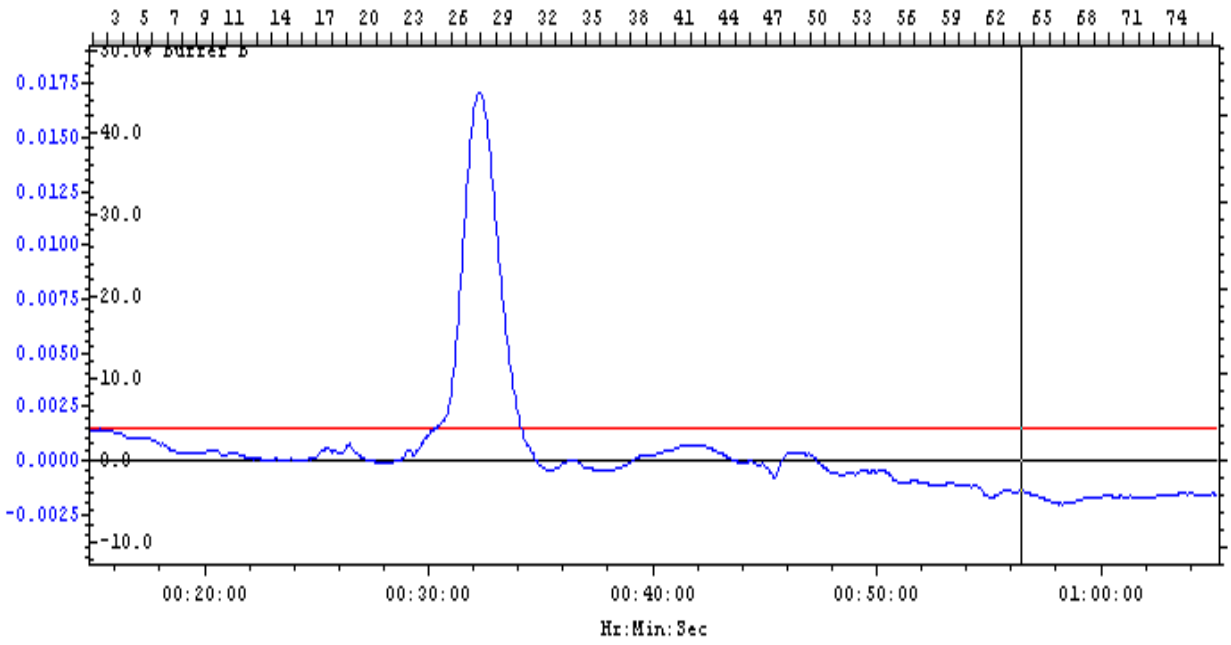

Figure 2. Gel-filtration chromatography analysis of AM.

2. Flow cytometry study

2.1 Assessment of *in vitro* binding specificity for the antigen receptor

Both Alexa dye-APSCA and Alexa dye-AM mAbs successfully bound to the antigens PSCA and mesothelin expressed on the tested cell lines. Flow cytometry analysis of T3M4-PSCA cells showed a high percentage of stained cells (78%), with a fluorescence intensity geometric mean value of 34, which is quite different from the 5.8 auto-fluorescence geometric mean value obtained for the untreated cells. Analysis of 293-Meso cells showed a higher percentage of stained cells (89%), even though the difference between the fluorescence intensity values of the stained 293-Meso cells (29) and the auto-fluorescence (1.6) was almost the same reported for T3M4-PSCA cells (see fig. 3). These results confirmed the ability of APSCA and AM to detect the antigens expressed on the cell surface.

Based on these results, we consider to use the same two cell lines to test the binding properties of radiolabeled APSCA and AM mAbs.

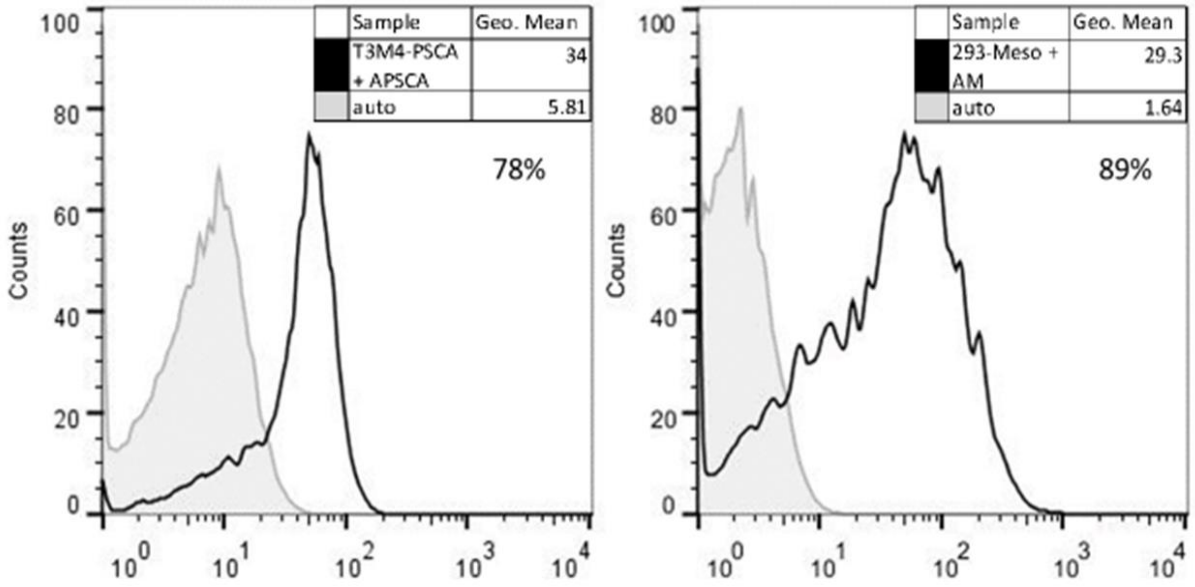

Figure 3. Flow cytometry study. Left panel shows T3M4-PSCA cells treated with dye-APSCA mAb (black) and untreated cells (grey plot); right panel shows 293-Meso cells treated with dye-AM mAb (black) and untreated cells (grey plot).

2.2 Assessment of *in vivo* binding specificity for the antigen receptor by optical imaging

A total body optical imaging scanning was carried out after intravenous injection of Alexa dye-mAbs on highly immunodeficient NOG mice bearing simultaneously Ag positive and negative tumors at two distinct sites; results showed that both mAbs tended to accumulate at either tumor sites during the first 24 h post-injection. Thereafter, the non-specific signal detectable in Ag-negative tumors progressively reduced, while the intensity of signals on Ag-positive masses constantly increased up to days 5-7 (see fig. 4).

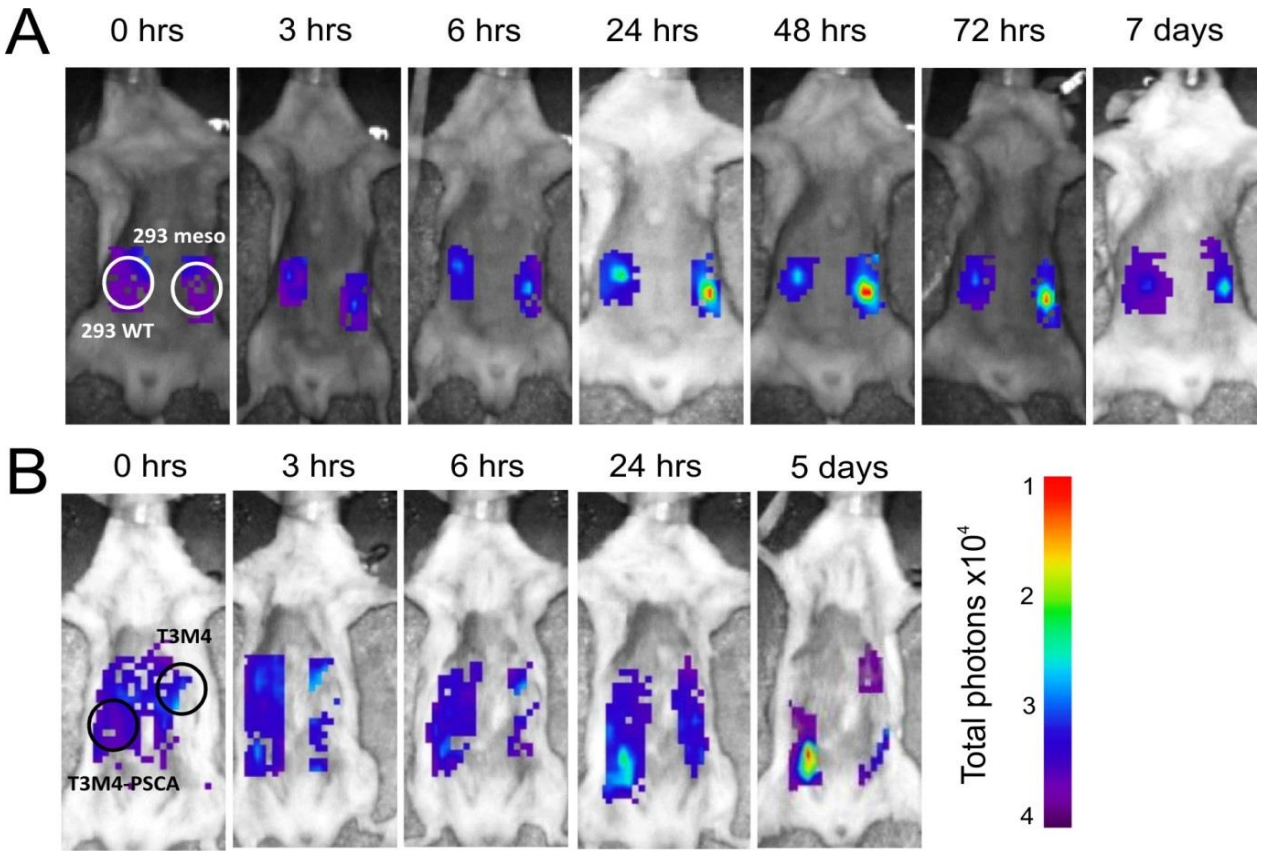

Figure 4. Assessment of in vivo binding specificity for the antigen receptor by optical imaging scanning at different time points, using A) 50 µg of Alexa dye-AM and B) 50 µg of Alexa dye-APSCA.

3. Direct labeling of mAbs

3.1 Reduction of mAbs

Direct labeling was carried out by addition of 2-ME to the mAbs to generate the sulfhydryl groups necessary to react with reduced ^{99m}Tc. As expected in this experiment, when the ratio of mAb:2-ME increased, the number of sulfhydryl groups per mAb increased.

Size exclusion HPLC UV-chromatogram of AM after reduction using a molar ratio 1:2000, presented a large peak at retention time of 9 min, which is quite similar to the retention time of unreduced AM (8.8 min). However, once the molar ratio increased to 1:2500, two smaller peaks with longer retention time (9.4 min and 13.8 min) were found. When the ratio further increased to 1:3500, the peaks became more significant and a peak at 10.6 min also appeared (see fig. 5). This fact denoted the presence of new species with lower molecular weight due

to the mAb degradation. Therefore, it was decided to use a molar ratio of 1:2000 to reduce the AM, since it was the highest ratio that did not produce degradation.

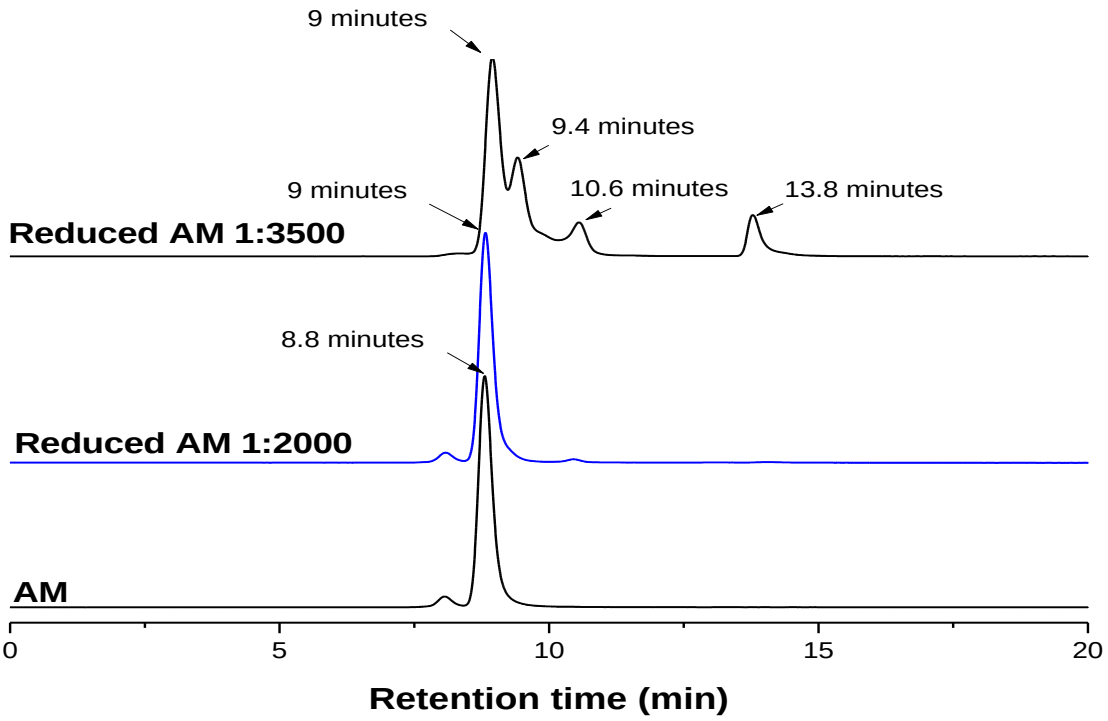

Figure 5. Size exclusion HPLC chromatograms at 280 nm of AM mAb, and reduced AM with 1:2000 and 1:3500 (mAb:2-ME) molar ratios.

APSCA mAb showed to be more resistant to the reduction. Size exclusion HPLC UV-chromatogram after incubation with 2-ME using a molar ratio of 1:3000 showed just one peak with a retention time (10 min) similar to the retention time of the unreduced-APSCA peak (9.7 min). However, when the molar ratio increased to 1:3500 APSCA mAb was quickly degraded. UV-chromatogram showed a small peak with shorter retention time, which suggested the formation of species with higher molecular weight as antibody aggregates, as well as two peaks with longer retention time (14.3 and 15.3 min) that indicated the creation of mAb fragments (see fig. 6). Thus, a molar ratio 1:3000 (mAb:2-ME) was selected to reduce the APSCA.

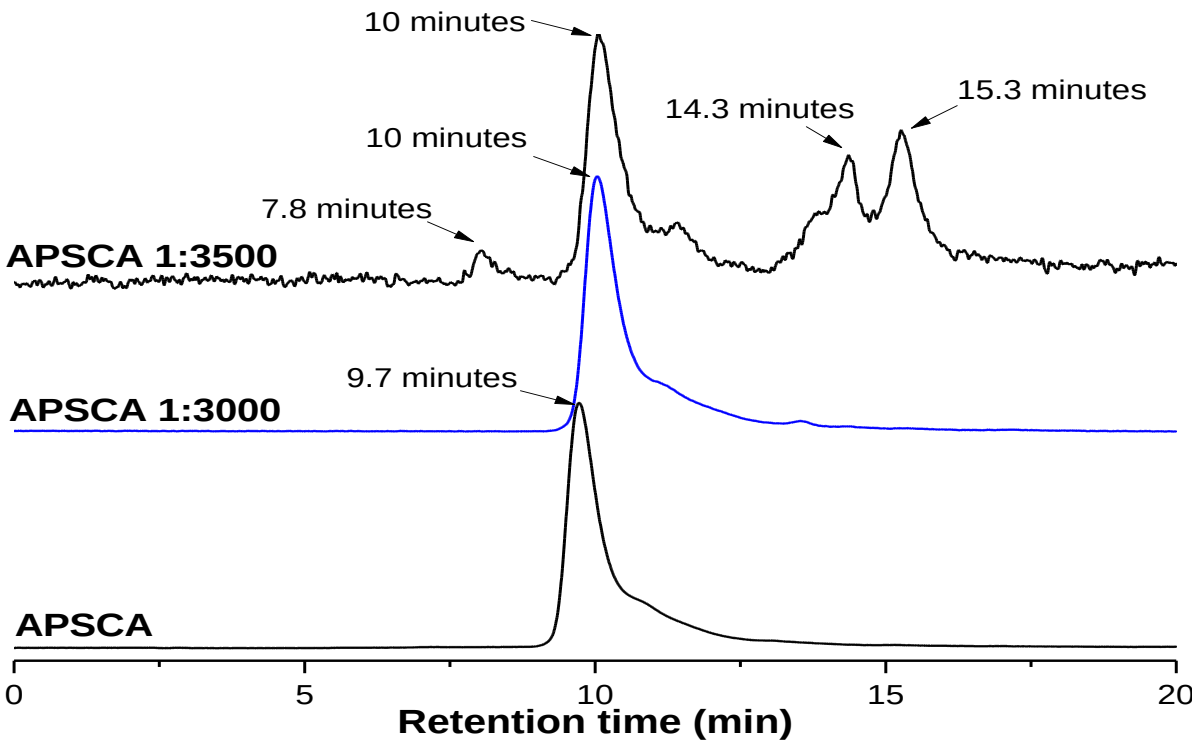

Figure 6. Size exclusion HPLC chromatograms at 280 nm showing APSCA mAb, and reduced APSCA with molar ratios 1:3000 and 1:3500 (mAb:2-ME)

Ellman's reaction test of reduced AM identified from 5 to 6 free sulfhydryl groups per mAb molecule, and 7 to 8 per each reduced APSCA. Consequently, the averages of free sulfhydryl groups out of the total number of thiol groups were 18 % and 25 % per each molecule of AM and APSCA, respectively. These percentages are appropriate, to obtain a high LE without causing mAb degradation as mentioned before. Results were in agreement with the data reported by Iznaga-Escobar *et al.*[83]. They obtained 5.5 and 6.6 free sulfhydryl group per each ior/cea1 and ior egf/e3 mAbs respectively, after the reduction with 2-ME using a 1:2000 molar ratio.

3.2 Labeling of mAbs with Technetium-99m (^{99m}Tc)

Different formulations were prepared and analyzed by size exclusion HPLC in order to select the one with the highest LE. The chromatographic profiles were obtained using two different detectors, the UV-Vis detector and a radiometric detector. Sample passes first by the UV-Vis

detector and 0.2 min (0.2ml, 1 ml/ml) later passes by the radio-detector. Correspondence of retention times of peaks of interest in the chromatogram is accepted as proof of the chemical identity of the compound. Radioactivity recovery was routinely determined to discard the presence of ^{99m}Tc-hydrolysed species or ^{99m}Tc-colloid which remains trapped in the column.

The volume of $^{99m}TcO_4^-$ solution is the factor that stated the final volume of the reaction mixture. The results demonstrated that 200 µL of $^{99m}TcO_4^-$ solution were enough to have a good labeling, while higher volumes of $^{99m}TcO_4^-$ (300 and 500 µL) produced a lower labeling yield for both mAbs. Concentration of reducing agent $SnCl_2$ was also assessed. Size exclusion HPLC-radiochromatogram of the product showed a small amount of $^{99m}TcO_4^-$ when 0.5 µg of $SnCl_2$ were added, which disappeared when the reduction agent was increased to 1 or 2 µg. No presence of colloids was found after recovery test in any case; however, we preferred to maintain the amount of $SnCl_2$ as low as possible to avoid any possibility of mAb degradation.

The effect of EHDP concentrations on the yield of ^{99m}Tc-mAbs was also studied; the results showed that even a small amount of EHDP (0.5 µg) was enough to reach its weak competition ligand function. Size exclusion HPLC-radiochromatograms showed a peak with a retention time of about 13 min, corresponding to the ^{99m}Tc-EHDP when a higher concentration was used.

After setting up the best reagents concentration and $^{99m}TcO_4^-$ solution volume, the last step was to optimize the reaction time. The results showed high labeling yields from 30 min, which did not increase with the time.

The best LE (> 97%) was obtained after 30 min when 200 µg of reduced AM or APSCA was incubated with 200 µl (100 MBq) of $^{99m}TcO_4^-$ solution, 0.5 µg EHDP and 1 µg $SnCl_2$. Under these conditions, the percentages of radiolabeled impurities as colloids and ^{99m}Tc-EHDP were less than 3%. Therefore, the post-labeling purification step could be avoided.

Figure 7 shows the size exclusion HPLC radiochromatogram of ^{99m}Tc-APSCA obtained with this formulation. Two peaks were found, a main peak with retention time of 9.9 min that matches with the APSCA retention time, and a very small peak with a retention time of 13.2 min corresponding to the ^{99m}Tc-EHDP; no presence of peak corresponding to $^{99m}TcO_4^-$ was found.

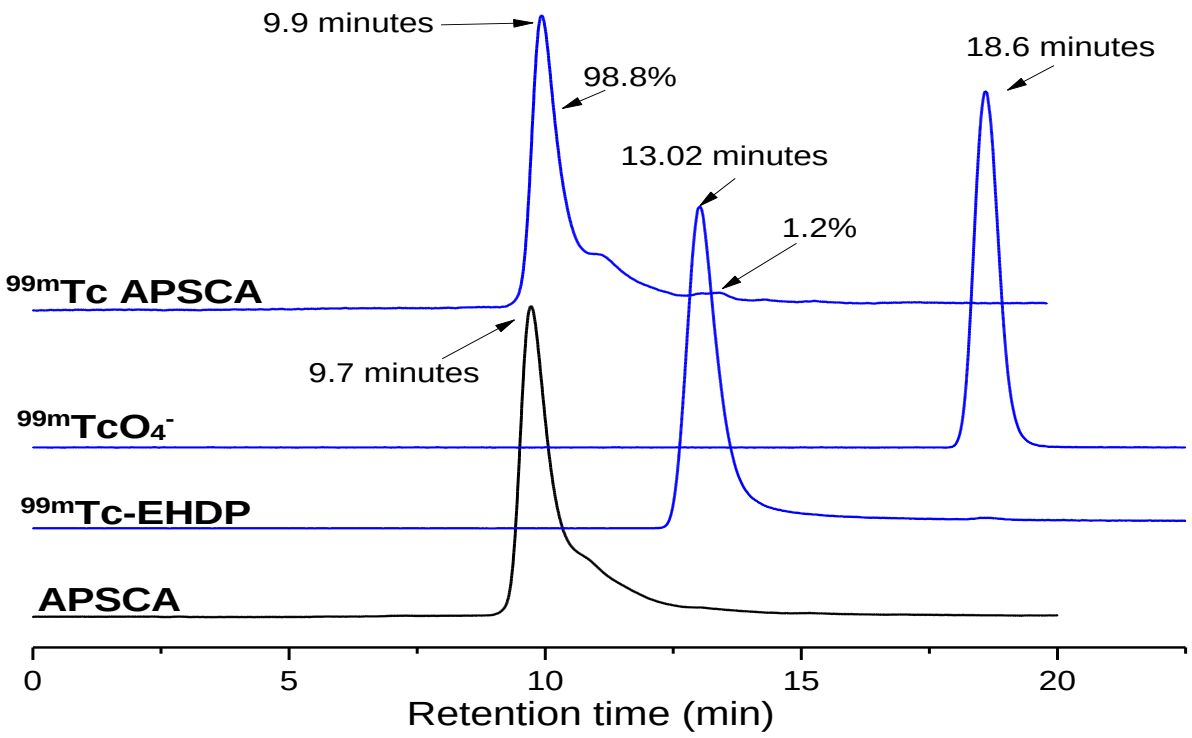

Figure 7. Size exclusion- UV HPLC chromatogram at 280 nm of APSCA (black line) and radiochromatograms of ^{99m}Tc APSCA, ^{99m}Tc-EHDP and $^{99m}TcO_4^-$ (blue lines).

^{99m}Tc-AM radiochromatogram showed similar results; a main peak with a retention time that fits the AM retention time, and a small peak corresponding to the ^{99m}Tc-EHDP; no presence of $^{99m}TcO_4^-$ was found (see fig. 8).

These results are similar to the data reported by A Bartolazzi et al. after ^{99m}Tc direct radiolabeling of a mAb against galectin-3[84]. They obtained a LE of 95% with the same labeling method but using 7 µl of methylen-diposphonate (MDP) bone scan kit which contained 0.5 µg of reducing agent stannous fluoride that might be not enough to reduce all free $^{99m}TcO_4^-$, and a high amount of the weak competitor medronate (7 µg) that could produce a small amount of ^{99m}Tc-medronate as contaminant. This might be the reason of why they reported a slight higher percentage of impurities (5 %) compared with our results (2 %).

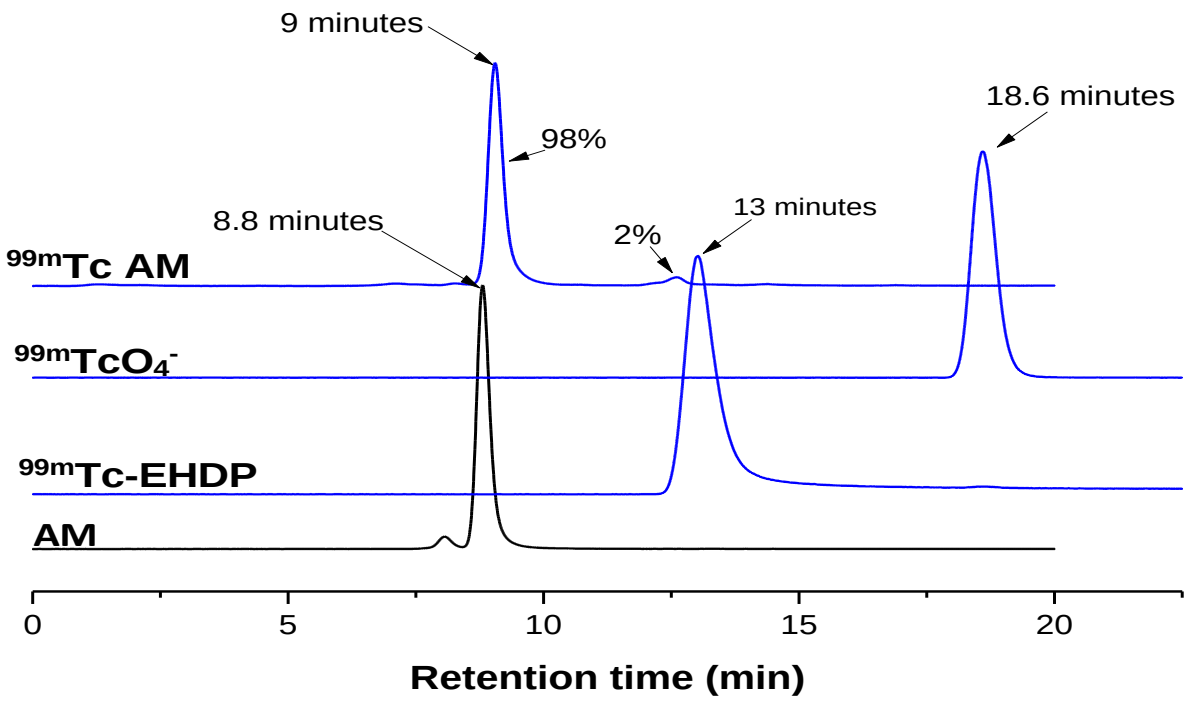

Figure 8. Size exclusion- UV HPLC chromatogram at 280 nm of AM (black line) and radiochromatograms of ^{99m}Tc AM ^{99m}Tc-EHDP and $^{99m}TcO_4^-$ (blue lines).

3.3 Stability studies of ^{99m}Tc-labeled mAbs

Dilution stability

^{99m}Tc-AM and ^{99m}Tc-APSCA stability was tested after dilution in SS, PBS or HS solutions. The results showed that both ^{99m}Tc-mAbs were quite stable. However, ^{99m}Tc-AM was more stable, its RCP being about 97% after 24 h incubation in the highest SS dilution (1:100) (see fig. 9A). RCP of ^{99m}Tc-APSCA was near 95% at the same conditions (see fig. 9B).

Stability after dilution with PBS was quite similar; the RCP after incubation at the dilution 1:100 for 24 h was higher for ^{99m}Tc-AM (97.5 %) than for ^{99m}Tc-APSCA (≈ 96 %) (see fig. 10).

The greatest instability was found after dilution in the HS. In this case, RCP decreased to 94% and 90% after 6 h incubation at a dilution of 1:10 for ^{99m}Tc-AM and ^{99m}Tc-APSCA, respectively (see fig.11). Size exclusion HPLC radiochromatograms of ^{99m}Tc-mAbs dilutions carried out 24h

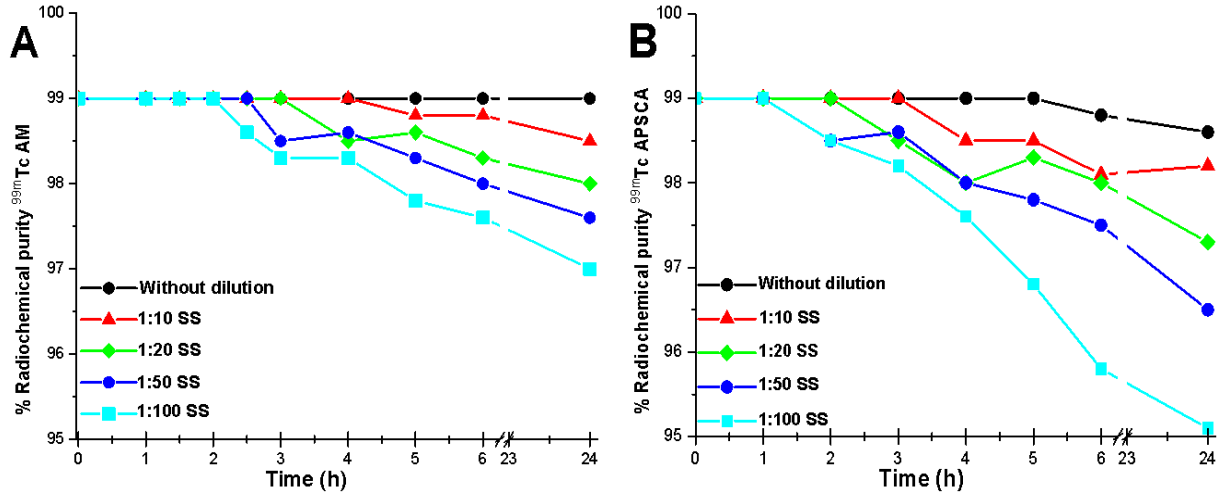

Figure 9. Percent of RCP after incubation at increasing dilutions of ^{99m}Tc-mAbs in SS at room temperature for 24 h. Panel A) refers to ^{99m}Tc-AM and panel B) to ^{99m}Tc APSCA.

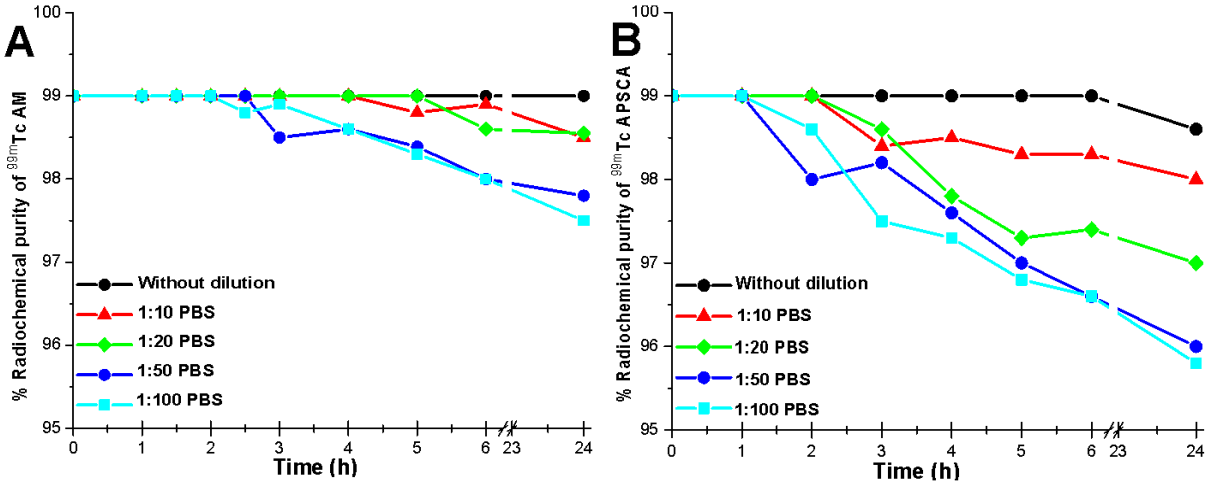

Figure 10. Percent of RCP after incubation at increasing dilutions of ^{99m}Tc-mAbs in PBS at room temperature for 24 h. Panel A) refers to ^{99m}Tc-AM and panel B) to ^{99m}Tc APSCA.

after incubation showed the creation of new small radioactive peaks corresponding to molecules with lower molecular weight. This fact indicated that a small percentage of mAb was degraded perhaps due to the enzymes present in the serum. These results are in agreement with the data reported by Malviya et al[85]. They used the same direct labeling method to obtain a ^{99m}Tc-1D09C3 mAb with a RCP of 85%, which decreased to 60% after six hours incubation at 37°C in a HS dilution 1:10.

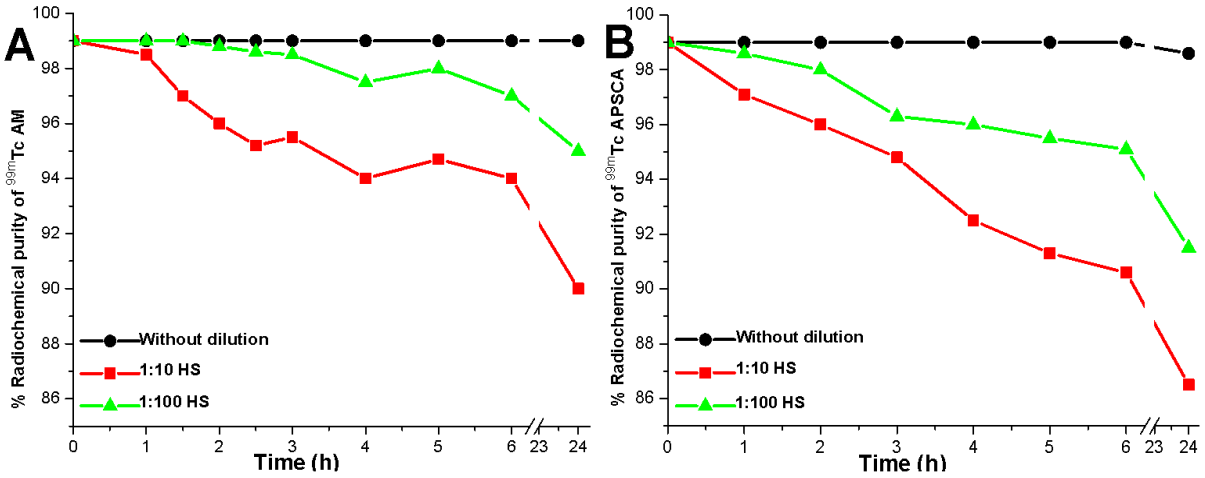

Figure 11. Percent of RCP after incubation at increasing dilutions of ^{99m}Tc-mAbs in HS for 24 h. Panel A) refers to ^{99m}Tc-AM and panel B) to ^{99m}Tc APSCA.

Cysteine challenge assay

Cysteine challenge assay determines the stability of ^{99m}Tc-mAb bonds in the presence of cysteine, and therefore it can be considered a good estimation of ^{99m}Tc-mAb *in vivo* stability. Both radiolabeled mAbs were quite stable toward transchelation with cysteine, RCP being more than 90% after 1h incubation at 1:100 (mAb:cysteine) molar ratio (see fig. 12). However, the results demonstrated that ^{99m}Tc-AM was less stable toward transchelation than ^{99m}Tc-APSCA, differently from the other stability studies.

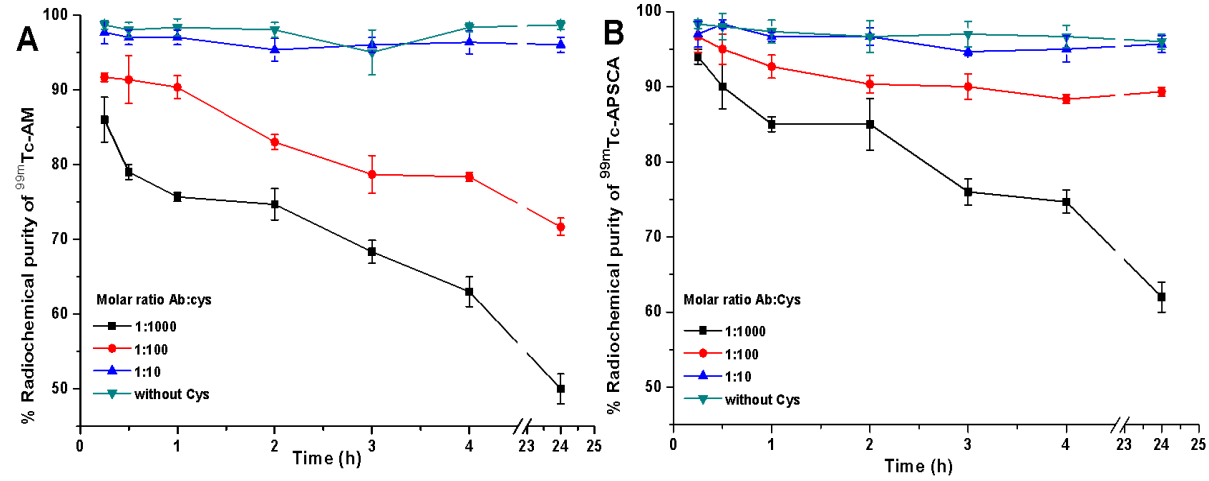

Figure 12. Percent of RCP after incubation of ^{99m}Tc-mAbs with cysteine solution using molar ratios 1:10, 1:100 and 1:1000 (mAb:cysteine). Panel A) refers to ^{99m}Tc-AM and panel B) to ^{99m}Tc APSCA

3.4 Assessment of ^{99m}Tc-mAbs binding specificity for the antigen receptor *in vitro*

^{99m}Tc-mAbs must maintain their ability to recognize specifically the antigens expressed on the cell surface, to be used as diagnostic agents. For this reason, cell uptake and internalization of ^{99m}Tc-labeled AM and APSCA mAbs were assessed by a competition binding assay using 293-Meso and T3M4-PSCA cell lines. Results showed that ^{99m}Tc-AM and ^{99m}Tc-APSCA non-specific binding (2.1% and 1.9%, respectively) was almost half of specific binding (4.6% and 3.4%, respectively), and a paired T-test calculation for both ^{99m}Tc-mAbs confirmed a statistically significant difference between unblocked and blocked cells, which demonstrated that in both cases labeled mAbs maintain the specific binding to the antigen expressed on the cell membrane (see fig. 13).

Percentage of internalization was calculated considering the total uptake as 100%. The results showed a 34% and 27% of internalization for ^{99m}Tc-AM and ^{99m}Tc-APSCA, respectively (see fig. 14); no difference between the internalization by blocked and unblocked cells was found for both ^{99m}Tc-mAbs, likely due to a same mechanism of internalization.

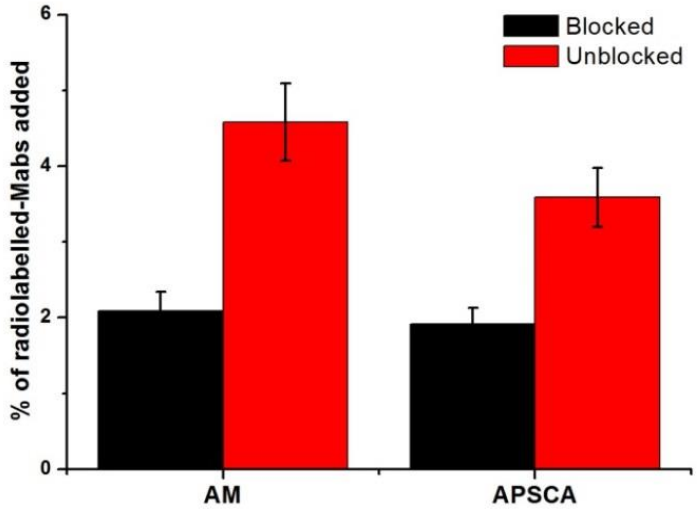

Figure 13. Percentage of ^{99m}Tc-AM and ^{99m}Tc-APSCA uptake on 293-Meso and T3M4-PSCA cells, respectively.

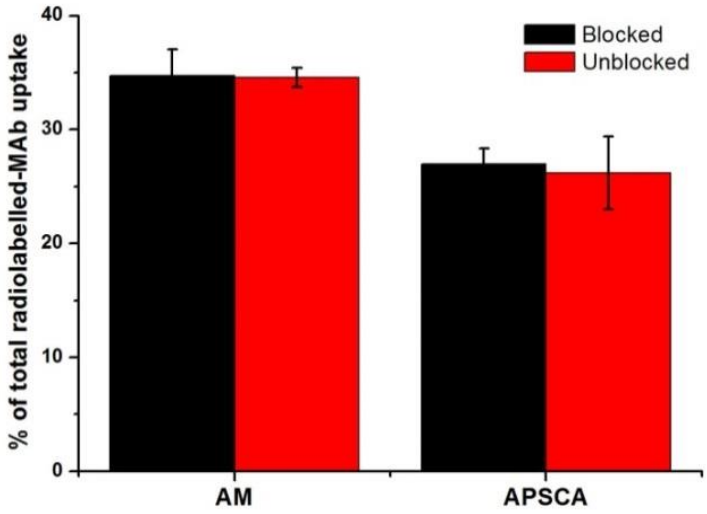

Figure 14. Percentage of ^{99m}Tc-AM and ^{99m}Tc-APSCA internalization on 293-Meso cells and T3M4-PSCA cells, respectively (considering the total uptake as 100%).

4. Indirect labeling of mAbs

4.1 Conjugation of chelating agent to mAbs

Size exclusion HPLC-chromatograms of DOTA-mAbs conjugates revealed the presence of a single product as result of the conjugation reactions; therefore, further purification was not necessary.

DOTA-APSCA conjugate chromatogram showed a peak with a shorter retention time (8.9 min) than the APSCA mAb retention time (9.7 min), this fact suggesting the formation of a structure with higher molecular weight (see fig.15A). Similar results were obtained for DOTA-AM conjugate where retention time for AM was 8.8 min, and 8.2 min for DOTA-AM. (See fig.15B).

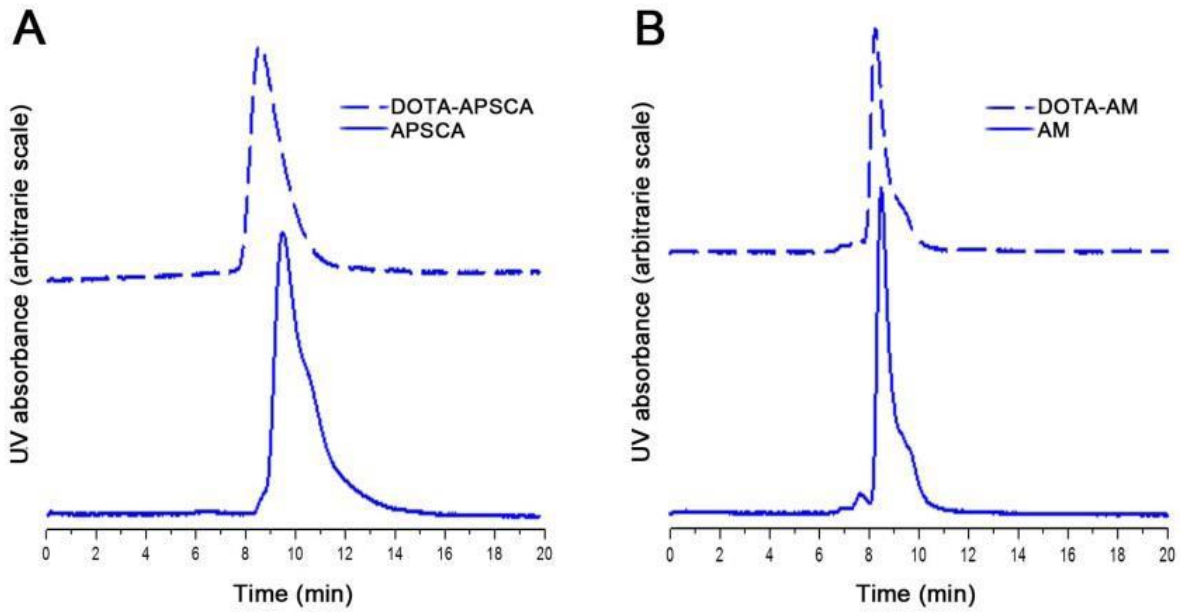

Figure 15. Size exclusion HPLC chromatograms of mAbs (280 nm) before conjugation (solid lines) and after DOTA conjugation (dashed lines). Panel A refers to APSCA and Panel B reports data for AM

4.2 Quantification of chelating agent number conjugated to each mAb molecule

MALDI-MS analysis of APSCA mAb solution showed a main peak of a mass-to charge ratio (m/z) of 150912 corresponding to unconjugated APSCA (see fig. 16A). MALDI-MS analysis of the APSCA mAb solution after the DOTA conjugation showed the main peak at 154067 (see fig. 16B). Therefore, DOTA-APSCA conjugates contained an average of 6 DOTA molecules per mAb, this number being calculated as the difference between APSCA and DOTA-APSCA main peaks (3155) divided by the mass of a single DOTA moiety (553).

MALDI-MS analysis of DOTA-AM conjugate and AM showed main peaks of m/z of 151895 and 149232, respectively (see fig. 17A and B). Applying the same method as before, an average of 5 DOTA molecules were calculated to be conjugated per each AM mAb molecule.

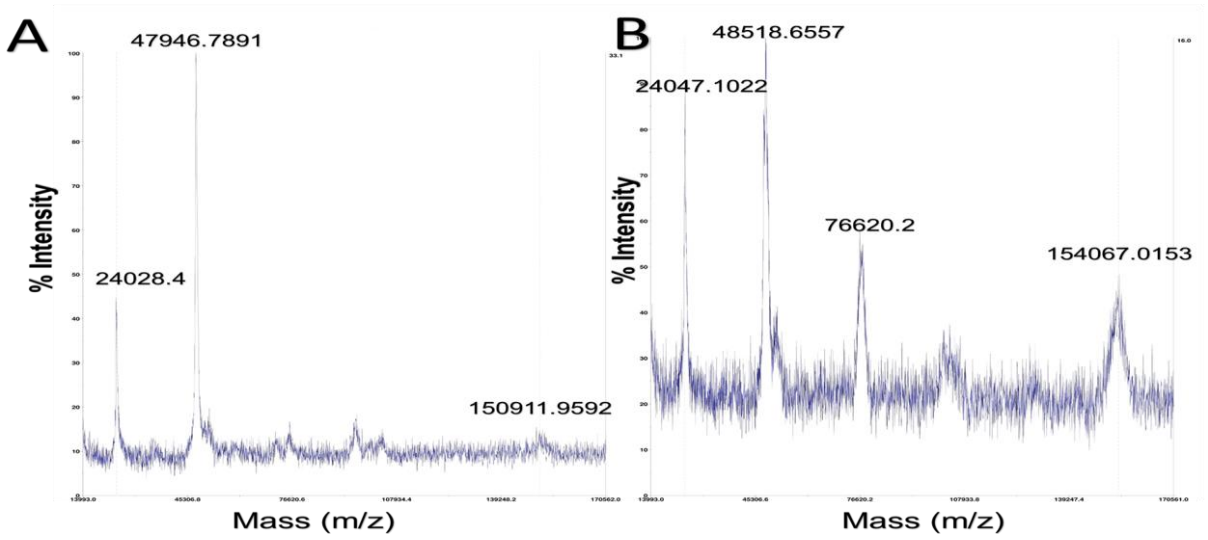

Figure 16. MALDI-MS spectra of A) unconjugated APSCA and B) $(DOTA)_6$-APSCA conjugate.

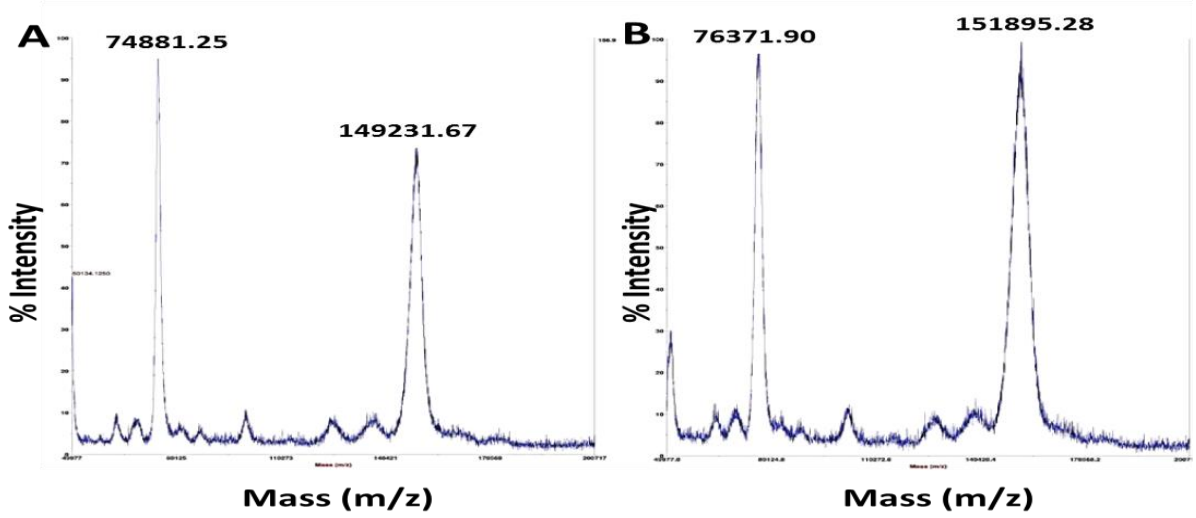

Figure 17. MALDI-MS spectra of A) unconjugated AM and B) $(DOTA)_5$-AM conjugate.

According to the data reported by Forrer et al, the number of DOTA molecules conjugated to the mAbs is enough in both cases to produce a therapeutic effect without affecting the immunoreactivity of the mAbs. Indeed, using the same labeling method to obtain ^{177}Lu-DOTA-anti-CD20, Forrer demonstrated that one conjugated DOTA molecule per mAb did not

produce therapeutic effects, but if the number increased to more than 8 DOTA per each mAb the immunoreactivity was dramatically reduce[82].

4.3 Assessment of DOTA-mAb binding specificity for the antigen receptor *in vitro*

DOTA-mAbs binding specificity tests were carried out by flow cytometry to study the effect of DOTA conjugation to the mAb immunoreactivity. Cytometry binding curves demonstrated that APSCA affinity for the receptor slightly decreased after DOTA conjugation (fig. 18). On the other hand, the reduction in AM mAb immunoreactivity was higher since the concentration of AM required to saturate half of the antigen receptors (IC50) decreased from 5 nM to 50 nM after DOTA conjugation (see fig. 18).

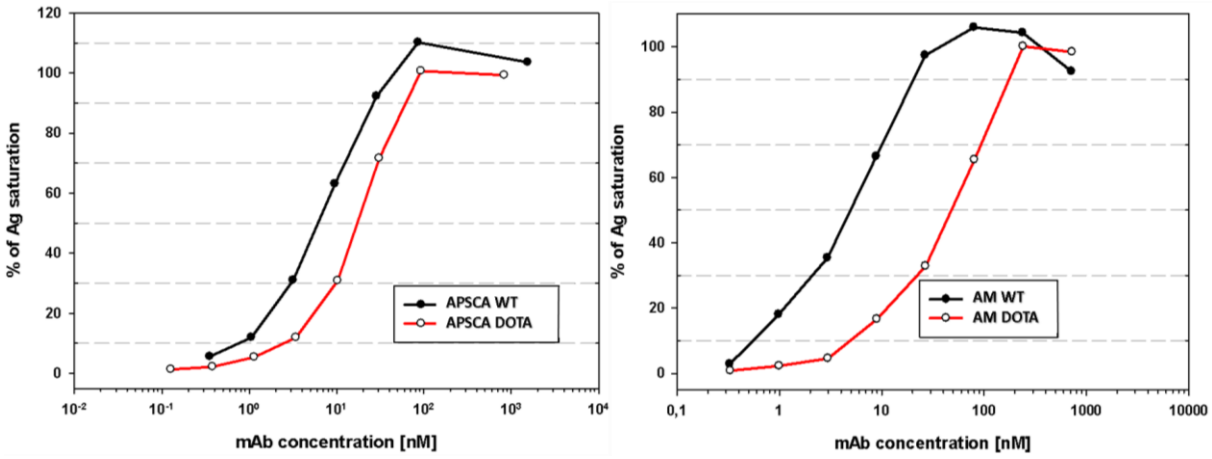

Figure 18. Flow cytometry binding analysis of unconjugated APSCA and $(DOTA)_6$-APSCA conjugate (left panel), and unconjugated AM and $(DOTA)_5$-AM conjugate (right panel).

4.4 Labeling of DOTA-mAb with Lutetium-177 (^{177}Lu)

High LE of DOTA-mAbs was found in both cases. Size exclusion HPLC and ITCL analyses showed that 68% and 52% of the reactivity was associated to DOTA-AM and DOTA-APSCA conjugates respectively, just 15 min after incubation. The LE increased to 95% for ^{177}Lu-DOTA-AM and 90% for ^{177}Lu-DOTA-APSCA after 1 h of incubation, and these values remained stable for 4 hours.

4.5 Stability studies of ^{177}Lu-labeled DOTA-mAb

Dilution stability

^{177}Lu-DOTA-AM and ^{177}Lu-DOTA-APSCA showed to be stable after dilution in SS or PBS for 6 h. However, ^{177}Lu-DOTA-APSCA size exclusion HPLC analysis showed a small peak with longer retention time that appeared after 6 h incubation and increased with the time until 24 h, possibly due to the degradation of the mAb (see fig. 19). ^{177}Lu-DOTA-AM proved to be more stable since size exclusion HPLC analysis of both dilutions showed a RCP higher than 95% even after 24 h of incubation (see fig. 19).

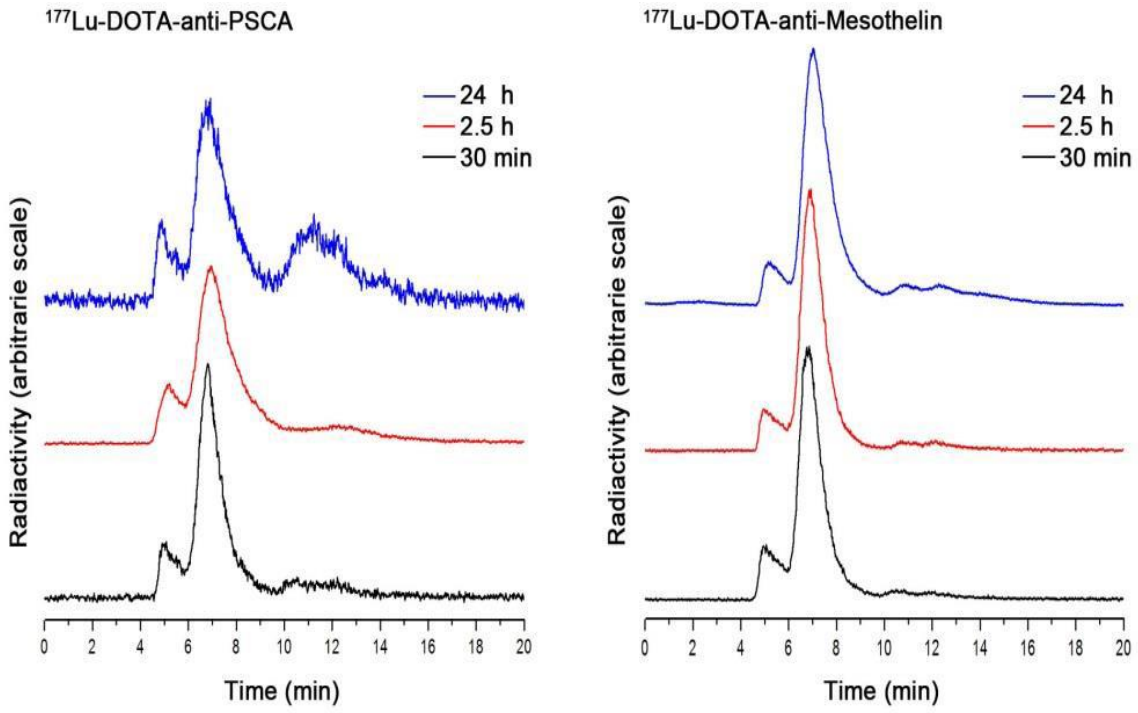

Figure 19. Size exclusion-radiochromatograms of ^{177}Lu-DOTA-APSCA (left panel) and ^{177}Lu-DOTA-AM (right panel) analyzed at different times for 24 h after dilution 1:100 in SS.

Stability against transchelation

Size exclusion HPLC analysis showed that there was no transchelation of ^{177}Lu from the labeled immunoconjugates to DTPA even after 3 days of incubation.

4.6 Assessment of ^{177}Lu-DOTA-mAbs binding specificity for the antigen receptor *in vitro*

^{177}Lu-DOTA-APSCA and ^{177}Lu-DOTA-AM specific bindings were 38% and 48% respectively, while their non-specific bindings were markedly lower (8% and 7%, respectively). Paired T-test demonstrated a statistically significant difference between the specific and non-specific bindings in both cases (see fig. 20).

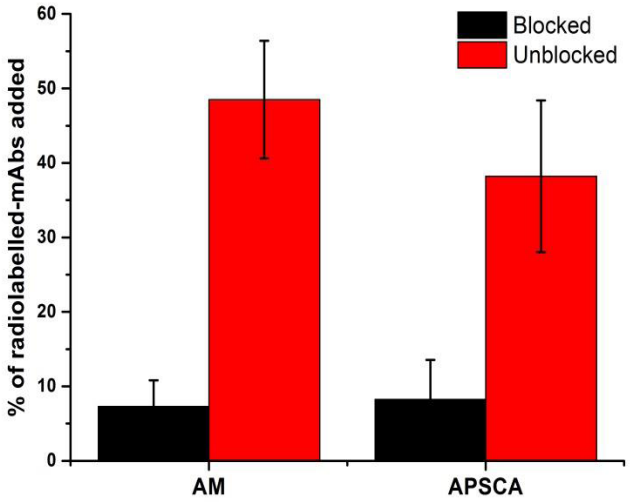

Figure 20. Uptake of ^{177}Lu-DOTA-AM and ^{177}Lu-DOTA-APSCA on 293-Meso and T3M4-PSCA cells respectively.

In this study, PSCA and mesothelin antigens were chosen as TAAs; both are specifically expressed on pancreatic cancer with nearly no expression on normal pancreatic tissues. These findings place APSCA and AM mAbs in a crucial position for diagnosis and therapy of pancreatic cancer[33,38,39,86].

First insights from flow cytometry studies carried on Ag+/- tumor cells confirmed the ability of our mAbs to detect the expression of PSCA and mesothelin TAAs on the surface of tested cells both *in vitro and in vivo*.

As mentioned before, targeting TAAs of pancreatic cancer by mAbs showed encouraging results in preclinical studies[87,88]. However, due to poor unpredictable vasculature of the desmoplastic ECM and heterogeneity of tumor specific antigens, clinical trials achievements ranged from disappointing results to modest clinical improvement[2,87]. The purpose of this project was therefore radiolabeling mAbs with γ and β^- emitter radionuclides to overcome these obstacles.

The underlying concept is supported by reports of other groups: APSCA mAb labeled with ^{125}I succeeded as a diagnostic tool for pancreatic cancer in a mouse model[40]. Likewise, AM mAb was able to detect pancreatic cancer primary and metastatic sites when labeled with ^{111}In in a clinical trial, or with ^{89}Zr in a mouse model[34,35]. However, this is the first time that either APSCA or AM are directly labeled with the γ emitter ^{99m}Tc to target pancreatic cancer. In the present study, both mAbs were directly labeled with ^{99m}Tc using EHDP as a weak competing ligand by preparation of different formulations to optimize EHDP and $SnCl_2$ concentrations, pH and reaction time. Direct radiolabeling gives rise to a high LE of > 97% with radiochemical impurities of < 3% and no free $^{99m}TcO_4^-$. Thus, post-labeling purification step was skipped. We also highlighted the high stability of both radiolabeled mAbs against dilution and transchelation, this latter being considered a good indicator for *in vivo* stability. In addition, the assessment of *in vitro* biological recognition of mAbs using Ag+/- tumor cells disclosed that mAbs specific binding to their corresponding TAAs was maintained after radiolabeling with ^{99m}Tc.

As previously reported, pancreatic cancer has hypovascular ECM and TAAs with heterogeneous distribution. To overcome the limited mAbs cytotoxic effect in this environment, our mAbs were radiolabeled with the ^{177}Lu radionuclide to take advantage of the β^- cross-fire effect. This is the first time that APSCA and AM mAbs are radiolabeled with ^{177}Lu to be used in pancreatic cancer.

In this setting, mAbs were radiolabeled with ^{177}Lu by indirect method using the macrocyclic chelating agent DOTA at a molar ratio of 1:5 (mAb:DOTA) and coupling buffer (pH 9.5), to increase the number of DOTA per each mAb molecule without affecting their immunoreactivity. Five or six DOTA molecules were obtained per each AM or APSCA molecule, respectively. In the following step, we successfully radiolabeled DOTA-mAbs with ^{177}Lu and obtained LE of 95% and 90% for ^{177}Lu-DOTA-AM and ^{177}Lu-DOTA-APSCA, respectively. Both radioimmunoconjugates showed stability against dilution and transchelation. However, ^{177}Lu-DOTA-AM showed higher stability than ^{177}Lu-DOTA-APSCA after dilution. These results are considered a good predictive factor regarding *in vivo* stability and biodistribution. Even though cytometry study demonstrated a reduction in mAbs binding affinity to their TAAs after DOTA conjugation, *in vitro* binding specificity study disclosed that ^{177}Lu-DOTA-AM and ^{177}Lu-DOTA-APSCA maintained their biological recognition for tumor cells, thus supporting their application as therapeutic agents for pancreatic cancer in future studies.

To conclude, AM and APSCA mAbs that efficiently detected pancreatic cancer cells *in vitro* and *in vivo* were successfully labeled using direct and indirect methods with ^{99m}Tc and ^{177}Lu, respectively. All the resulting compounds were prepared by rapid simple methods and demonstrated high RCP, high *in vitro* stability and high *in vitro* binding specificity. Therefore, our results are highly encouraging and open additional opportunities for further *in vivo* studies to assess such mAbs as novel imaging diagnostic and effective therapeutic tools in pancreatic cancer.

Abbreviations

Prostatic stem cell antigen	PSCA
Tumor-associated antigens	TAAs
Anti-PSCA	APSCA
Anti-Mesothelin	AM
Monoclonal antibodies	mAbs
Positron	β^+
Gamma	γ
Technetium-99m	^{99m}Tc
Labeling efficiency	LE
Quality of life	QoL
Beta$^-$	β^-
Lutetium-177	^{177}Lu
1,4,7,10-tetraazacyclododecane-1,4,7,10-tetraacetic acid	DOTA
Overall survival	OS
Pancreatic ductal adenocarcinoma	PDAC
Carbohydrate antigen 19-9	CA 19-9
Computed tomography	CT
Magnetic resonance imaging	MRI
Ultrasonography	US
Positron emission tomography	PET
Performance status	PS
Gemcitabine	GEM

Intensity-modulated radiation therapy	IMRT
Extracellular matrix	ECM
Transforming growth factor- β	TGF-β
Epithelial mesenchymal transition	EMT
Carcinoembryonic antigen	CEA
Colorectal cancer	CRC
Gastrointestinal tract	GIT
Secreted glycoprotein acidic and rich in cysteine	SPARK
Food and Drug Administration	FDA
Zirconium-89	^{89}Zr
Indium-111	^{111}In
Glycosylphosphatidylinositol	GPI
Renal cell carcinoma	RCC
Iodine-*	$^{*}I$
Single photon emission tomography	SPECT
Interleukin-2	IL-2
Tumor necrosis factors	TNF
Chronic lymphocytic leukaemia	CLL
Non-Hodgkin´s lymphoma	NHL
Epidermal growth factor receptor	EGFR
Squamous cell carcinoma of head and neck	SCCHN
Non-small cell lung cancer	NSCLC
Human epidermal growth factor receptor-2	HER2
Vascular endothelial growth factor receptor-2	VEGFR-2
Receptor activator of nuclear factor kappa-B ligand	RANK-L
Cytotoxic associated T lumphocyte protein	4 CTLA-4

Programmed death ligand 1	PD-L1
Antibody-dependent cellular cytotoxicity	ADCC
Complement mediated cytotoxicity	CMC
Fluorine-18	^{18}F
Alpha	α
Linear energy transfer	LET
Deoxyribonucleic acid	DNA
Isometric transition	IT
Electron capture	ec
Tin (II) chloride	$SnCl_2$
Bifunctional chelating agent	BFCA
Diethylenetriaminepentaacetic acid	DTPA
1,4,7-triazacyclononane-1,4,7-triacetic acid	NOTA
Gallium	Ga
1,4,8,11 tetraazacyclotetradecane, 1,4,8,11,tetraacetic acid	TETA
Copper	Cu
Sodium iodide	NaI
Thallium-doped sodium iodide	Tl
Photo-Multiplier tubes	PMT
Molybdenum-99	^{99}Mo
Radioimmunotherapy	RIT
Yttrium-90	^{90}Y
Fetal bovine serum	FBS
Phosphate buffer solution	PBS
Three dimensional	3D
High Performance Liquid Chromatography	HPLC

Ultra violet	UV
2-mercaptoethanol	2-ME
Etidronic acid solution	EHDP
Saline chloride solution	SS
Human serum	HS
Radiochemical purity	RCP
Instant thin layer chromatography analysis	ITLC
Silica gel	SG
Retention factor	Rf
Matrix-assisted laser desorption ionization mass spectroscopy	MALDI-MS
Fluorescein isothiocyanate	FITC
Fluorescence-activated cell sorting	FACS
Methylen-diposphonate	MDP

Bibliography

1. Zhang Q, Zeng L, Chen Y, et al. Pancreatic Cancer Epidemiology, Detection, and Management. Gastroenterology Research and Practice. 2016;2016:8962321.

2. Blanco VM, Latif T, Chu ZT, Qi XY. Imaging and Therapy of Pancreatic Cancer with Phosphatidylserine-Targeted Nanovesicles. Translational Oncology. 2015;8(3):196-203.

3. Wolfgang CL, Herman JM, Laheru DA, et al. Recent progress in pancreatic cancer. Ca-a Cancer Journal for Clinicians. 2013;63(5):318-348.

4. Jones S, Zhang XS, Parsons DW, et al. Core signaling pathways in human pancreatic cancers revealed by global genomic analyses. Science. 2008;321(5897):1801-1806.

5. Biankin AV, Waddell N, Kassahn KS, et al. Pancreatic cancer genomes reveal aberrations in axon guidance pathway genes. Nature. 2012;491(7424):399-405.

6. Yachida S, Jones S, Bozic I, et al. Distant metastasis occurs late during the genetic evolution of pancreatic cancer. Nature. 2010;467(7319):1114-U1126.

7. Mayr M, Schmid RM. Pancreatic cancer and depression: myth and truth. BMC Cancer. 2010;10:569.

8. Ducreux M, Cuhna AS, Caramella C, et al. Cancer of the pancreas: ESMO Clinical Practice Guidelines for diagnosis, treatment and follow-up(aEuro). Annals of Oncology. 2015;26:V56-V68.

9. Varadhachary GR, Tamm EP, Abbruzzese JL, et al. Borderline resectable pancreatic cancer: Definitions, management, and role of preoperative therapy. Annals of Surgical Oncology. 2006;13(8):1035-1046.

10. Suker M, Beumer BR, Sadot E, et al. FOLFIRINOX for locally advanced pancreatic cancer: a systematic review and patient-level meta-analysis. Lancet Oncol. 2016;17(6):801-810.

11. Neesse A, Michl P, Frese KK, et al. Stromal biology and therapy in pancreatic cancer. Gut. 2011;60(6):861-868.

12. Weber CE, Kuo PC. The tumor microenvironment. Surgical Oncology-Oxford. 2012;21(3):172-177.

13. Subhash VV, Yeo MS, Tan WL, Yong WP. Strategies and Advancements in Harnessing the Immune System for Gastric Cancer Immunotherapy. Journal of Immunology Research. 2015.

14. Amedei A, Niccolai E, D'Elios AM. T Cells and Adoptive Immunotherapy: Recent Developments and Future Prospects in Gastrointestinal Oncology. Clinical & Developmental Immunology. 2011.

15. Masamune A, Shimosegawa T. Pancreatic stellate cells--multi-functional cells in the pancreas. Pancreatology. 2013;13(2):102-105.

16. Mahadevan D, Von Hoff DD. Tumor-stroma interactions in pancreatic ductal adenocarcinoma. Molecular Cancer Therapeutics. 2007;6(4):1186-1197.

17. Kyuno D, Yamaguchi H, Ito T, et al. Targeting tight junctions during epithelial to mesenchymal transition in human pancreatic cancer. World Journal of Gastroenterology. 2014;20(31):10813-10824.

18. Toole BP, Slomiany MG. Hyaluronan: A constitutive regulator of chemoresistance and malignancy in cancer cells. Seminars in Cancer Biology. 2008;18(4):244-250.

19. Seicean A, Petrusel L, Seicean R. New targeted therapies in pancreatic cancer. World Journal of Gastroenterology. 2015;21(20):6127-6145.

20. Shi JX, Qin JJ, Ye H, Wang P, Wang KJ, Zhang JY. Tumor associated antigens or anti-TAA autoantibodies as biomarkers in the diagnosis of ovarian cancer: a systematic review with meta-analysis. Expert Rev Mol Diagn. 2015;15(6):829-852.

21. Zhang J-Y, Looi KS, Tan EM. Identification of tumor-associated antigens (TAAs) as diagnostic and predictive biomarkers in cancer. Methods in molecular biology (Clifton, N.J.). 2009;520:1-10.

22. Hollstein M, Sidransky D, Vogelstein B, Harris CC. p53 mutations in human cancers. Science. 1991;253(5015):49-53.

23. Zhang JY, Chan EK, Peng XX, et al. Autoimmune responses to mRNA binding proteins p62 and Koc in diverse malignancies. Clin Immunol. 2001;100(2):149-156.

24. Scanlan MJ, Gure AO, Jungbluth AA, Old LJ, Chen YT. Cancer/testis antigens: an expanding family of targets for cancer immunotherapy. Immunol Rev. 2002;188:22-32.

25. Vigneron N. Human tumor antigens and cancer immunotherapy. BioMed research international. 2015;2015.

26. Tan EM, Zhang J. Autoantibodies to tumor-associated antigens: reporters from the immune system. Immunol Rev. 2008;222:328-340.

27. Glenn J, Steinberg WM, Kurtzman SH, Steinberg SM, Sindelar WF. EVALUATION OF THE UTILITY OF A RADIOIMMUNOASSAY FOR SERUM CA-19-9 LEVELS IN PATIENTS BEFORE AND AFTER TREATMENT OF CARCINOMA OF THE PANCREAS. Journal of Clinical Oncology. 1988;6(3):462-468.

28. Ansari D, Aronsson L, Sasor A, et al. The role of quantitative mass spectrometry in the discovery of pancreatic cancer biomarkers for translational science. Journal of Translational Medicine. 2014;12.

29. Neuzillet C, Tijeras-Raballand A, Cros J, Faivre S, Hammel P, Raymond E. Stromal expression of SPARC in pancreatic adenocarcinoma. Cancer Metastasis Rev. 2013;32(3-4):585-602.

30. Pastan I, Hassan R. Discovery of Mesothelin and Exploiting it as a Target for Immunotherapy. Cancer research. 2014;74(11):2907-2912.

31. Morello A, Sadelain M, Adusumilli PS. Mesothelin-Targeted CARs: Driving T cells to Solid Tumors. Cancer discovery. 2016;6(2):133-146.

32. Ordonez NG. Application of mesothelin immunostaining in tumor diagnosis. American Journal of Surgical Pathology. 2003;27(11):1418-1428.

33. Argani P, Iacobuzio-Donahue C, Ryu B, et al. Mesothelin is overexpressed in the vast majority of ductal adenocarcinomas of the pancreas: Identification of a new pancreatic cancer marker by serial analysis of gene expression (SAGE). Clinical Cancer Research. 2001;7(12):3862-3868.

34. Lindenberg L, Thomas A, Adler S, et al. Safety and biodistribution of 111In-amatuximab in patients with mesothelin expressing cancers using single photon emission computed tomography-computed tomography (SPECT-CT) imaging. Oncotarget. 2015;6(6):4496-4504.

35. ter Weele EJ, van Scheltinga AGTT, Kosterink JGW, et al. Imaging the distribution of an antibody-drug conjugate constituent targeting mesothelin with (89)Zr and IRDye 800CW in mice bearing human pancreatic tumor xenografts. Oncotarget. 2015;6(39):42081-42090.

36. Saeki N, Gu JA, Yoshida T, Wu XF. Prostate Stem Cell Antigen: A Jekyll and Hyde Molecule? Clinical Cancer Research. 2010;16(14):3533-3538.

37. Reiter RE, Gu ZN, Watabe T, et al. Prostate stem cell antigen: A cell surface marker overexpressed in prostate cancer. Proceedings of the National Academy of Sciences of the United States of America. 1998;95(4):1735-1740.

38. Argani P, Rosty C, Reiter RE, et al. Discovery of new markers of cancer through serial analysis of gene expression: Prostate stem cell antigen is overexpressed in pancreatic adenocarcinoma. Cancer Research. 2001;61(11):4320-4324.
39. Wente MN, Jain A, Kono E, et al. Prostate stem cell antigen is a putative target for immunotherapy in pancreatic cancer. Pancreas. 2005;31(2):119-125.
40. Foss CA, Fox JJ, Feldmann G, et al. Radiolabeled anti-claudin 4 and anti-prostate stem cell antigen: Initial imaging in experimental models of pancreatic cancer. Molecular Imaging. 2007;6(2):131-139.
41. Dougan M, Dranoff G. Immune Therapy for Cancer. Annual Review of Immunology. 2009;27:83-117.
42. Kershaw MH, Teng MWL, Smyth MJ, Darcy PK. Supernatural T cells: Genetic modification of T cells for cancer therapy. Nature Reviews Immunology. 2005;5(12):928-940.
43. Weiner GJ. Monoclonal antibody mechanisms of action in cancer. Immunologic Research. 2007;39(1-3):271-278.
44. Sarko D, Eisenhut M, Haberkorn U, Mier W. Bifunctional chelators in the design and application of radiopharmaceuticals for oncological diseases. Curr Med Chem. 2012;19(17):2667-2688.
45. Carvalho S, Levi-Schaffer F, Sela M, Yarden Y. Immunotherapy of cancer: from monoclonal to oligoclonal cocktails of anti-cancer antibodies: IUPHAR Review 18. British Journal of Pharmacology. 2016;173(9):1407-1424.
46. Carter P. Improving the efficacy of antibody-based cancer therapies. Nat Rev Cancer. 2001;1(2):118-129.
47. Clark M. Antibody humanization: a case of the 'Emperor's new clothes'? Immunol Today. 2000;21(8):397-402.
48. Scott AM, Wolchok JD, Old LJ. Antibody therapy of cancer. Nat Rev Cancer. 2012;12(4):278-287.
49. Young K, Smyth E, Chau I. Ramucirumab for advanced gastric cancer or gastro-oesophageal junction adenocarcinoma. Therapeutic Advances in Gastroenterology. 2015;8(6):373-383.
50. Guglielmi AP, Sobrero AF. Second-Line Therapy for Advanced Colorectal Cancer. Gastrointestinal Cancer Research : GCR. 2007;1(2):57-63.
51. Fani M, Maecke HR. Radiopharmaceutical development of radiolabelled peptides. Eur J Nucl Med Mol Imaging. 2012;39 Suppl 1:S11-30.
52. Claesson AK, Stenerlow B, Jacobsson L, Elmroth K. Relative biological effectiveness of the alpha-particle emitter (211)At for double-strand break induction in human fibroblasts. Radiat Res. 2007;167(3):312-318.
53. Kassis AI, Adelstein SJ. Radiobiologic principles in radionuclide therapy. J Nucl Med. 2005;46 Suppl 1:4s-12s.
54. Sharkey RM, Goldenberg DM. Targeted therapy of cancer: New prospects for antibodies and immunoconjugates. Ca-a Cancer Journal for Clinicians. 2006;56(4):226-243.
55. Adelstein SJ, Kassis AI, Bodei L, Mariani G. Radiotoxicity of iodine-125 and other auger-electron-emitting radionuclides: background to therapy. Cancer Biother Radiopharm. 2003;18(3):301-316.
56. Clarke SEM. RADIONUCLIDE THERAPY OF THE THYROID. European Journal of Nuclear Medicine. 1991;18(12):984-991.
57. Carlsson J, Aronsson EF, Hietala SA, Stigbrand T, Tennvall J. Tumour therapy with radionuclides: assessment of progress and problems. Radiotherapy and Oncology. 2003;66(2):107-111.

58. Kawashima H. Radioimmunotherapy: a specific treatment protocol for cancer by cytotoxic radioisotopes conjugated to antibodies. ScientificWorldJournal. 2014;2014:492061.
59. Handbook of Radiopharmaceuticals: Wiley; 2003.
60. Liu S. Bifunctional coupling agents for radiolabeling of biornolecules and target-specific delivery of metallic radionuclides. Advanced Drug Delivery Reviews. 2008;60(12):1347-1370.
61. Gansow OA, Brechbiel MW, Mirzadeh S, Colcher D, Roselli M. Chelates and antibodies: current methods and new directions. Cancer Treat Res. 1990;51:153-171.
62. Lee S, Xie J, Chen X. Peptides and peptide hormones for molecular imaging and disease diagnosis. Chem Rev. 2010;110(5):3087-3111.
63. Heppeler A, Froidevaux S, Macke HR, et al. Radiometal-labelled macrocyclic chelator-derivatised somatostatin analogue with superb tumour-targeting properties and potential for receptor-mediated internal radiotherapy. Chemistry-a European Journal. 1999;5(7):1974-1981.
64. Figueiras FP, Jimenez X, Pareto D, Gispert JD. Partial Volume Correction using an Energy Multiresolution Analysis. presented at: IEEE Nuclear Science Symposium Conference 2009; Oct 25-31, 2009; Orlando, FL.
65. Bateman TM. Advantages and disadvantages of PET and SPECT in a busy clinical practice. J Nucl Cardiol. 2012;19 Suppl 1:S3-11.
66. Kunjachan S, Ehling J, Storm G, Kiessling F, Lammers T. Non-invasive Imaging of Nanomedicines and Nanotheranostics: Principles, Progress and Prospects. Chemical reviews. 2015;115(19):10907-10937.
67. Del Sordo S, Abbene L, Caroli E, Mancini AM, Zappettini A, Ubertini P. Progress in the Development of CdTe and CdZnTe Semiconductor Radiation Detectors for Astrophysical and Medical Applications. Sensors. 2009;9(5):3491-3526.
68. Fukumoto M. Single-photon agents for tumor imaging: 201Tl, 99mTc-MIBI, and 99mTc-tetrofosmin. Ann Nucl Med. 2004;18(2):79-95.
69. Fakhar-E-Alam M, Roohi S, Atif M, Firdous S, Amir N, Zahoor R. Labelling and optimization of PHOTOFRIN (R) with Tc-99m. Radiochimica Acta. 2010;98(12):813-818.
70. Wang AY, Lin JL, Lin WC. Studies on the porphine labeled with Tc-99m-pertechnetate. Journal of Radioanalytical and Nuclear Chemistry. 2010;284(1):21-28.
71. Prise KM, O'Sullivan JM. Radiation-induced bystander signalling in cancer therapy. Nat Rev Cancer. 2009;9(5):351-360.
72. Kroemer G, Galluzzi L, Brenner C. Mitochondrial membrane permeabilization in cell death. Physiological Reviews. 2007;87(1):99-163.
73. Cabon L, Galan-Malo P, Bouharrour A, et al. BID regulates AIF-mediated caspase-independent necroptosis by promoting BAX activation. Cell Death and Differentiation. 2012;19(2):245-256.
74. Cutler CS, Smith CJ, Ehrhardt GJ, Tyler TT, Jurisson SS, Deutsch E. Current and potential therapeutic uses of lanthanide radioisotopes. Cancer Biother Radiopharm. 2000;15(6):531-545.
75. Stein R, Chen S, Haim S, Goldenberg DM. Advantage of yttrium-90-labeled over iodine-131-labeled monoclonal antibodies in the treatment of a human lung carcinoma xenograft. Cancer. 1997;80(12):2636-2641.
76. Wahl RL. Tositumomab and (131)I therapy in non-Hodgkin's lymphoma. J Nucl Med. 2005;46 Suppl 1:128s-140s.
77. SJ M, David E. Reduction-mediated technetium-99m labeling of monoclonal antibodies . Vol 31. J. Nucl. Med.1990.

78. Malviya G, de Vries EF, Dierckx RA, Signore A. Synthesis and evaluation of 99mTc-labelled monoclonal antibody 1D09C3 for molecular imaging of major histocompatibility complex class II protein expression. Mol Imaging Biol. 2011;13(5):930-939.
79. Soto Y, Mesa N, Alfonso Y, et al. Targeting arterial wall sulfated glycosaminoglycans in rabbit atherosclerosis with a mouse/human chimeric antibody. MAbs. 2014;6(5):1340-1346.
80. Al-Yasi AR, Carroll MJ, Ellison D, et al. Axillary node status in breast cancer patients prior to surgery by imaging with Tc-99m humanised anti-PEM monoclonal antibody, hHMFG1. Br J Cancer. 2002;86(6):870-878.
81. Mather SJ, Ellison D. REDUCTION-MEDIATED TC-99M LABELING OF MONOCLONAL-ANTIBODIES. Journal of Nuclear Medicine. 1990;31(5):692-697.
82. Forrer F, Chen J, Fani M, et al. In vitro characterization of Lu-177-radiolabelled chimeric anti-CD20 monoclonal antibody and a preliminary dosimetry study. European Journal of Nuclear Medicine and Molecular Imaging. 2009;36(9):1443-1452.
83. Iznaga Escobar N, Morales A, Nunez G. Micromethod for quantification of SH groups generated after reduction of monoclonal antibodies. Nucl Med Biol. 1996;23(5):641-644.
84. Bartolazzi A, D'Alessandria C, Parisella MG, et al. Thyroid Cancer Imaging In Vivo by Targeting the Anti-Apoptotic Molecule Galectin-3. PLoS ONE. 2008;3(11):e3768.
85. Malviya G, de Vries EFJ, Dierckx RA, Signore A. Synthesis and Evaluation of Tc-99m-Labelled Monoclonal Antibody 1D09C3 for Molecular Imaging of Major Histocompatibility Complex Class II Protein Expression. Molecular Imaging and Biology. 2011;13(5):930-939.
86. McCarthy DM, Maitra A, Argani P, et al. Novel markers of pancreatic adenocarcinoma in fine-needle aspiration: mesothelin and prostate stem cell antigen labeling increases accuracy in cytologically borderline cases. Appl Immunohistochem Mol Morphol. 2003;11(3):238-243.
87. Chames P, Kerfelec B, Baty D. Therapeutic Antibodies for the Treatment of Pancreatic Cancer. Thescientificworldjournal. 2010;10:1107-1120.
88. Hassan R, Ebel W, Routhier EL, et al. Preclinical evaluation of MORAb-009, a chimeric antibody targeting tumor-associated mesothelin. Cancer Immun. 2007;7:20.

ACKNOWLEDGEMENTS

I would like to express my sincere gratitude to the director of school **Prof. Paola Zanovello** and my Supervisor **Prof. Antonio Rosato** for welcoming me when I came Italy and for the help, support and motivation they gave me during my PhD program. I also want to thank **Dr.ssa Laura Melendez Alafort** for her precious support, knowledge and time that helped me finishing my thesis.